Facultad
de
Ciencias

Predicting the future Pulsar Wind Nebulae population in the TeV sky

(Prediciendo la futura población de nebulosas de púlsares en el cielo TeV)

Trabajo de Fin de Grado
Para acceder al

GRADO EN FÍSICA

Autor: Javier Gómez de la Gándara Pérez
Directora: Silvia Martínez Núñez (IFCA)
Co-Directora: Alison Mitchell (University of Zurich)

Julio - 2020

Agradecimientos

En primer lugar, me gustaría dar las gracias a mis padres por haberse sacrificado y haberme apoyado en todo momento durante estos 5 años de carrera. De igual manera a mis hermanos, por ser un apoyo para mí y espero haber sido un ejemplo para vosotros. Querría hacer mención a mi abuelo Braulio, con el que comparto la pasión por las matemáticas y la física, y mi abuela Fide, todos ellos fundamentales para mí.

También querría dar las gracias a mis primeros profesores de física en los Escolapios, que me abrieron las puertas a esta rama de la ciencia tan bonita (y no tan bonita en muchas ocasiones), como son Chema, Mario o Noelia.

A mis directoras, primero Silvia por haber aceptado adaptar este trabajo a principios del curso pasado (¡y vaya si se ha adaptado!) con el trabajo que ello conllevaba, más aún con la situación por la que todos hemos pasado como ha sido la cuarentena. Muchas gracias por tu apoyo y actitud. También a Alison, directora inicial del proyecto cuando se realizó durante el verano de 2019 en Zúrich. Llegué como un estudiante sin conocimientos ni de Python ni de púlsares y Alison fue de gran ayuda, siempre dispuesta a guiarme y a ayudarme. También quería darle las gracias por aceptar seguir ayudándonos a Silvia y a mí durante este curso, siendo clave su apoyo para que este trabajo haya salido adelante.

En último lugar, a mis compañeros y amigos que he hecho durante la carrera sin los cuales estos 5 años no hubiesen sido lo mismo. A mis amigos de la facultad, tanto de Física, Matemáticas o los intensos del doble grado, por nuestras aventuras y anécdotas tanto dentro como fuera de la facultad. En general, a todo aquel con el que haya pasado buenos momentos, ya sea en clase, en la biblioteca o en la cafetería. Si empiezo a nombraros a todos no termino. Con todos vosotros esta carrera se ha hecho mucho más amena y divertida, dentro de lo que cabe. También quiero mencionar a María, por haberme apoyado durante este año, con todo el tiempo que me ha quitado el TFG. Asimismo a mis amigos fuera de la facultad, a quiénes tampoco les he podido dedicar todo el tiempo que me gustaría. Por último, me gustaría mencionar a mis amigos durante mi Erasmus en Londres y mis prácticas en Zúrich, sin duda hicieron que vivir lejos de casa mereciese la pena y tenga un gran recuerdo de estas dos experiencias universitarias.

Abstract

The large amount of pulsars without TeV detected Pulsar Wind Nebulae (PWNe) has been a subject of interest in recent years. Although some pulsars have possible PWNe candidates at TeV energies, only a small fraction of them have been firmly identified with PWNe, meaning there is still much to be achieved in this field. Mainly all pulsars have been detected at radio frequencies so this project aims to predict future detections of PWNe at higher energies, more precisely, gamma-rays at $\gtrsim 1$ TeV. In order to accomplish it, a computational analysis of pulsars taken from the ATNF (Australia Telescope National Facility) pulsar catalogue has been carried out with the first purpose of studying their main properties, such as period, characteristic age or spin-down luminosity, where different samples of pulsars have been drawn. After defining our PWN evolutionary model we were able to predict PWNe features such as energy density, flux or angular size. Analysing these properties we have highlighted a list of candidate pulsars for future TeV detections which will be tracked down by the Cherenkov Telescope Array (CTA). Finally we have made a predicted map of PWNe lying in the Milky Way's galactic plane at 1 TeV energies and a halo source study for old PWNe.
The research part of this project has been performed during a summer fellowship program at the University of Zurich in 2019.

Key words: pulsar, Pulsar Wind Nebula (PWN),γ-ray astronomy, CTA, ATNF, halo.

Resumen

La gran cantidad de púlsares sin nebulosa aparente se ha convertido en un tema de interés durante los últimos años. Algunos púlsares tienen posibles candidatos de nebulosas de púlsares (NP) para energías de TeV, pero solo una pequeña parte de ellos han sido identificados con certeza, indicando que todavía hay mucho por descubrir en este campo. La mayoría de púlsares se han detectado en frecuencias de radio, por lo que este trabajo tiene como objetivo predecir futuras detecciones de NP en más altas energías, más concretamente, rayos gamma de $\gtrsim 1$ TeV. Para ello, se ha realizado un análisis computacional de púlsares recopilados del Catálogo de Púlsares del ATNF (infraestructura nacional de telescopios de Australia), con el primer propósito de estudiar sus principales propiedades como el periodo, edad o luminosidad, a partir de varias muestras. Tras definir nuestro modelo para la evolución de las NP, pudimos predecir sus características fundamentales, como la densidad de energía, el flujo o el tamaño angular. Analizando estas propiedades se ha obtenido una lista de púlsares candidatos para ser detectados en energías de TeV en un futuro gracias a CTA (red de telescopios Cherenkov). Por último, se ha realizado un mapa en coordenadas galácticas con el brillo superficial y el tamaño angular estimado de las NP que podrían ser detectadas en 1 TeV y un estudio sobre halos en NP más viejas.
La parte de investigación de este trabajo se ha realizado durante una estancia de verano en la Universidad de Zúrich en 2019.

Palabras clave: púlsar, nebulosa de púlsar, astronomía de rayos γ, CTA, ATNF, halo.

Contents

Chapter 1

Introduction

Pulsars are cosmic tools for scientists to study the matter in extreme conditions. The electromagnetic radiation emitted by pulsars carries information about these astronomical objects and what occurs inside them. This means pulsars can give us information about the physics of neutron stars, the densest material in the universe except for black holes. Considered as the most *natural clocks* in the universe, thanks to their very accurate rotation period, magnitudes like cosmic distances can be measured. Among their applications, multiple experiments are at this moment searching for gravitational waves by checking possible disruptions in their periods or their use to test aspects of Einstein's GR theory. In conclusion, pulsars are a current optimal instrument in terms of research and there is still a lot of progress to be done in this field.

1.1. The discovery of pulsars

Radio pulsars were discovered by Hewish and Bell in 1967 [1] studying the fluctuating radio signals of compact radio sources at low radio frequencies. Jocelyn Bell, Hewish's graduate student, discovered a strange source consisting apparently of scintillating radio signals in its entirety. After several surveys they found the signal consisted completely of a series of pulses with a period approximate of 1.33 s. This was the source PSR 1919+21, the first pulsar identified. The periodic signals obtained from this pulsar can be appreciated in Figure 1.1.

Pulsars were soon firmly identified with isolated, rotating, magnetised neutron stars, thanks to the very stable and short period of their pulses and polarised radio emission observed. To observe these pulses, the magnetic axis of the star and the rotation axis must be misaligned and then pulses originate from beams emitted along the magnetic axis [2].

Among the discovered pulsars, the young one in the Crab Nebula is of special interest. Known as PSR J0534+2200, or simply as the Crab, it has a high luminosity and since it is not too far away it can be studied in great detail. The short period of the Crab pulsar, 33 ms, led to conclude neutron stars as the parent bodies of radio pulsars, excluding any other possible body to originate them [2]. It was also found the derived age of the Crab

- around 1257 years - is consistent with the age of the remnant, recorded by Chinese astronomers in 1054 and corresponding to a true age of 966 years. This proved, together with other pulsars, that neutron stars are formed in supernova explosions. Another well-known pulsar is Geminga. Characterised by its very low distance, still uncertain, it is a very old pulsar with a large nebula size. Therefore it is thought Geminga interferes in the search of other sources. Besides, it is the only invisible pulsar in radio.

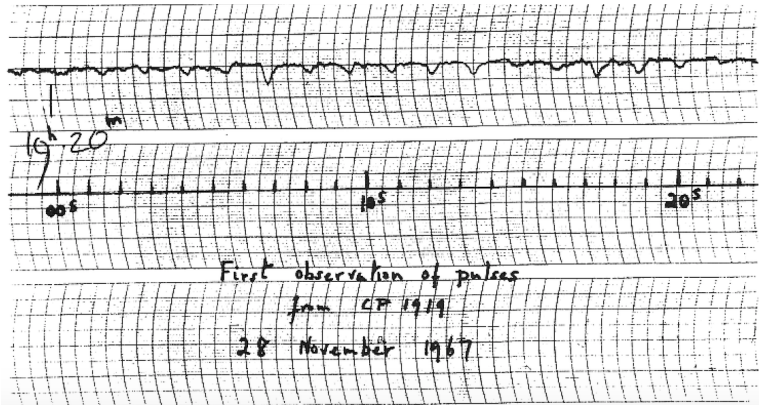

Figure 1.1: Signals of the first pulsar detected PSR 1919+21. Source: [1].

1.2. The origin of pulsars

Two of the main processes in a star are gravity and nuclear fusion. While the first one compresses the star to the center, what holds a star up and prevents it from collapsing is the second one, due to the thermal pressure. More precisely, radiation and thermal pressure of hot gas from nuclear energy generation in their central region expands the star layers outwards. Moreover, in any layer of a star there is a balance between gravity and thermal pressure, known as hydrostatic equilibrium [2].

Nuclear processing continues in all the stellar evolution process until the core of the star runs out of nuclear fuel and at this stage, with no more thermal pressure acting as the outward force, the star starts to collapse due to its own gravity. Figure 1.2 shows the different evolutionary journeys of a protostar depending on its initial mass. Possible equilibrium configurations which can exist at the end of the life cycle are white dwarfs, neutron stars or black holes.

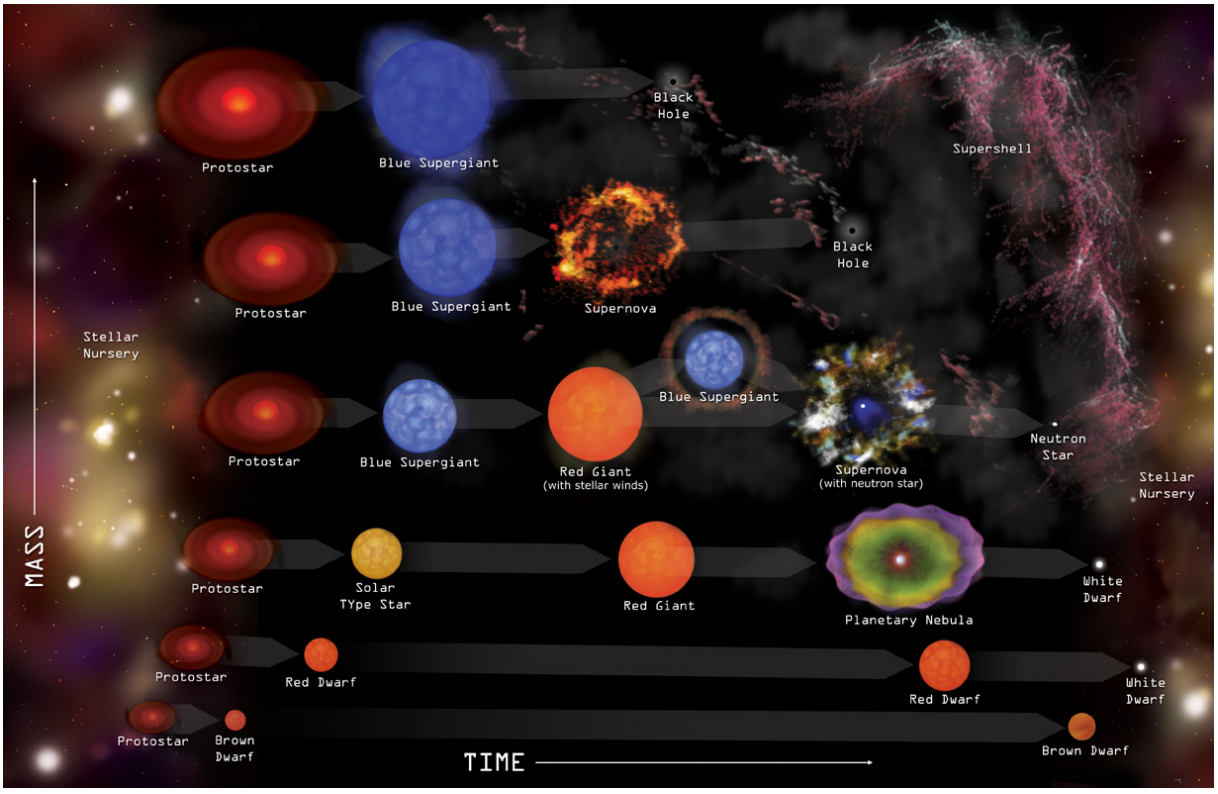

Figure 1.2: Stellar evolution of stars based on the initial mass of the star. Source [3].

On the formation of neutron stars there is a rapid liberation of huge amounts of energy. To shed some light on this process, the time scale for collapse of the iron core of a massive star is a few seconds. During a supernova (SN) the star explodes, the outer layers (the envelope) are ejected and this expulsion results in the formation of a supernova remnant (SNR). In addition to these layers, in the SNR there is interstellar material that is swept up and shocks along the way. The supernova explosion ejects part of the stellar material with supersonic speeds around 30,000 km/s, creating a shock wave ahead of the ejecta. Temperature raises up to millions of K and the shock starts to slow down at the same time it sweeps up the interstellar medium at a very low rate, requiring even thousands of years until its speed reaches the speed of sound.

However, this process is not very common, with only five supernovae observed during the last millennium within our Galaxy [2], although the number of supernova could be greater since many of them could be not visible due to the dust or being too far away to the current facilities. One of well-known supernovae is SN 1054, a very important SNR which gave rise to the Crab Nebula. Figure 1.3 shows an image of this nebula obtained by multi-wavelength observations, ranging from X-ray (Chandra Telescope) to radio (VLA).

Figure 1.3: Crab Nebula combined image from 5 different telescopes. Each colour represents a different observation: radio corresponds with the red coloured shell, yellow to infrared, green to visible, blue to ultraviolet and purple to X-ray. Source: [4].

1.3. Pulsar formation

When a neutron star is formed from the explosion of a supernova, the core of the preexisting star is violently compressed. Conservation of angular momentum $L = I\omega$, where $I \propto MR^2$ is the moment of inertia, accounts for its rapid rotation. Since the radius R of the core is reduced after the explosion up to 5-10 km (typical NS radius values) its angular velocity ω drastically increases. This is the reason why pulsars have typically very high angular rotational speed [5].

The core of the pulsar is electrically charged since not all protons and electrons are converted into neutrons during this violent compression, and thanks to the fast rotation, a strong varying magnetic field is created. Therefore electromagnetic radiation is produced towards the magnetic poles, but from the fact that the axis of rotation and magnetic poles are not aligned, which is one main feature of pulsars, we see a light pulse periodically [5]. Magnetic flux $\phi \propto BR^2$ conservation plays an important role here. Following the same idea, size reduction results in a sharp raise in the magnetic field B.

A light cylinder is created, centered on the pulsar and aligned with the rotation axis, with a radius such that particles at this radius have a rotating speed equal to the speed of light. Particles at first are trapped on the closed field lines and co-rotate. Due to this huge magnetic field, charged particles are accelerated to relativistic speeds, creating pulsar

winds which start at the light cylinder. This is shown schematically in Figure 1.4. The pulsar wind, after reaching that speed, can get into the surrounding interstellar medium (ISM), creating a shock wave called "wind termination shock", where the expanding wind slows to sound speed of medium. In conclusion, matter is decelerated [6].

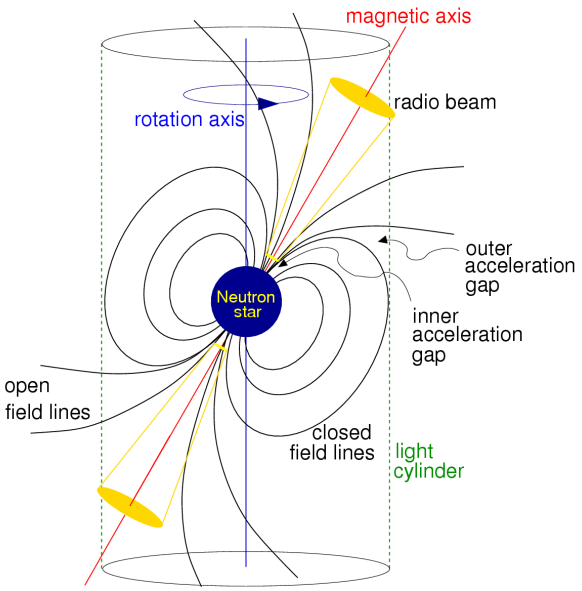

Figure 1.4: Scheme of the Light cylinder. The misalignment of both rotation and magnetic axis can be appreciated. Source: [6].

The magnetic axis of the neutron star is tilted with respect to the rotation axis. Very high energy charged particles that travel along the magnetic field lines close to the poles produce emission which is emitted in the direction of the field lines. While the neutron star is rotating, radiation from the beam sweeps across the Earth, generating a pulse each time it rotates, or even two pulses per rotation if the beams from both poles sweep past the Earth.

However, it must be remarked that there are many unanswered questions related to the process where the high energetic particles produce the radiation.

1.4. Pulsar Wind Nebulae

The size of the zone within which a pulsar's influence is dominant is called Pulsar Wind Nebula (PWN) and is mainly dictated by the external pressure and injected energy [7]. They are clouds of magnetised electron-positron plasma, usually observed via their synchrotron or inverse Compton radiation (IC) and are created in the SNR due to the high energetic wind of the pulsar interacting with its environment. Sometimes a PWN is surrounded by a SNR and in those cases, if we cannot distinguish them, the system is called composite.

A pulsar releases in its entire life around 10^{50} erg, where 1 erg is equivalent to 10^{-7} J. However, roughly 10 % of that energy is emitted as pulsar electromagnetic (EM) radiation. While a huge percent is radiated, mainly as synchrotron radiation, a small portion of the PWN energy is converted to IC radiation in the TeV band. Although it has just been stated that IC radiation is not one of the main emissions, it carries information that the synchrotron emission does not tell us, giving us a more general and complete idea of the electron population, in comparison with the synchrotron photons. Synchrotron emission usually comes from high energy electrons, in contrast with IC, also related to lower energies.

The lifetime of pulsars is usually around 10^5 or 10^6 kyr. Due to the continuous decrease of their magnetic and particle outflow, however, nearly all of the observed TeV PWNe come from pulsars with lifetime less than a few 100 kyr [8].

Inside the population of TeV sources, there is a fraction called TeV halos. A halo can be considered as an over-density of relativistic electrons around a source, here a PWNe, in a zone in which the source does not dominate the dynamics of the ISM. In fact, it is diffusion what is always expected to dominate in halos. They can only exist around the PWNe once electrons have started to escape in the ISM [8].

1.5. Pulsar wind evolution

This section consists of a brief introduction on the main evolutionary stages of a PWN, centering on the principal physical properties of the region where TeV emission is originated. In order to study the evolution of a PWN, the common formalism applied is magneto - hydrodynamics, where for young pulsars the confinement within the PWN is very effective.

Figure 1.5 shows three stages, split into ages, first $t \lesssim 10$ kyr, then the range $10 - 100$ kyr and $t \gtrsim 100$ kyr to conclude. Unless it is otherwise specified, in this section the term "electrons" will mean both electrons and positrons.

Stage 1: $\lesssim$ 10 kyr

During this stage, the pulsar is near its place of birth. The ejecta from the SN spreads out in the ISM, creating a forward shock. After its birth, the pulsar can receive an initial velocity - meaning it does not stay at its birthplace and can therefore move its position over time.
Then a reverse shock (RS) appears between the ejecta and the ISM while the expansion scales down but at this stage the RS has not reached the PWN yet. At some point, the RS turns back inwards to the centre, but since the SNR expands at a slower rate in the direction where the ISM density is higher, the RS might reach the PWN before in some directions than in others. Stage 1 finishes when the reverse shock breaks and reaches the PWN.

Stage 2: $\sim$ 10-100 kyr

At this point the morphology of the PWN-SNR system is irregular. As we can observe in Figure 1.5, the nebula is disturbed and the pulsar can be not centered with respect to the PWN. At this moment, the high-energy electrons commence to escape from the PWN, propagating to the surrounding SNR and even some of them can escape into the ISM.

Stage 3: $\gtrsim$ 100 kyr

During these late times, the pulsar has completely escaped from its parent SNR, which is still expanding at a very slow rate. The pulsar continues propagating in the ISM. As in the previous stage, high-energy electrons can escape into the ISM too.

However, it is at this point when TeV emission can be considered as a TeV halo, under the assumption that escaped relativistic electrons do not dominate the ISM energy density. It must be remarked only old PWNe, with $t \gtrsim 100$ kyr may be surrounded with TeV halos. X-ray and TeV sizes depend on the synchroton radiation producing particle population, while the TeV size, R_{TeV} is related to the population experiencing IC scattering. At young times of a PWN, X-ray and TeV emission have a comparable size, while for later times (from stage 2) its discrepancy becomes significant due to the production of TeV emission from IC scattering of lower energies cooled particles.

We have considered high energy electrons and positrons that produce TeV emission are accelerated at the same rate, but recent research found a pulsar may prefer a net charge at very high energies, instead of equal rates of electrons and positrons.

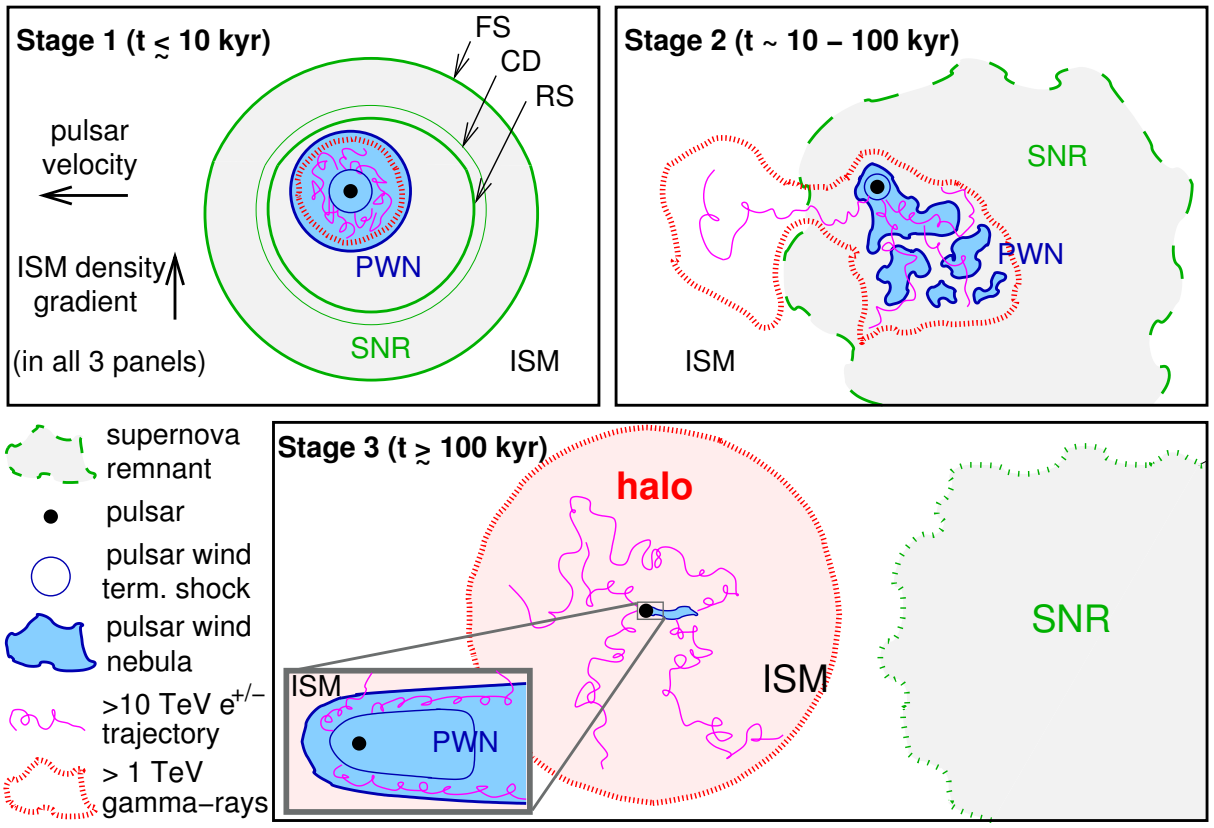

Figure 1.5: PWN evolution stages. At 1st stage the PWN is inside the SNR. When the reverse shock reaches the PWN and electrons start to get out from the PWN into the SNR, we enter into stage 2. At stage 3 the pulsar has escaped from the SNR, and high-energy electrons, in the ISM, may form a TeV Halo. FS stands for Forward Shock and RS the reverse shock. Reproduced with permission from [7].

1.6. Gamma-ray observations

Cosmic rays are atomic particles, mainly high-energy (HE) protons and atomic nuclei, accelerated to exceptionally high energies. With velocities very close to the speed of light, they are constantly arriving to the Earth. Cosmic rays were discovered by Victor Hess in 1912 and their spectrum covers a wide energy range, from the order of 10^9 eV (GeV) up to about 10^{20} eV.

Gamma rays are produced in the interactions of cosmic rays and provide the most accurate method to study them once they arrive to the Earth. Pulsars, PWNe and SNRs are the main galactic sources of HE γ rays, whose domain corresponds to photons with energies greater than 0.5 MeV. The most energetic cosmic photons presently detected are around 100 TeV.

Focusing on gamma rays production, we highlight two different processes. The first one is the interaction of HE electrons and positrons with radiation fields, producing synchroton photons at low energy gamma rays. But at this stage these photons can interact with

ambient low energy photons and boost them to very high energies (VHE) via IC scattering. These interactions are said to be leptonic processes. The second way of production occurs in denser regions of the ISM, where HE protons and nuclei interact with matter via nuclear interactions and mesons both charged and neutral are produced. Among these mesons, the neutral pions π^0 decay into γ rays. These processes involving nucleons and mesons are known as hadronic [9].

While HE astrophysics require space-based experiments since the atmosphere is opaque to photons beyond the optical waveband, the VHE domain, greater than 100 GeV, requires ground-based detectors and different techniques. Known as Imaging Atmospheric Cherenkov Telescopes (IACT), there are currently four operating facilities, the High Energy Stereoscopic System (HESS), Major Atmospheric Gamma Imaging Cherenkov Telescopes (MAGIC), First G-APD Cherenkov Telescope (FACT), and Very Energetic Radiation Imaging Telescope Array System (VERITAS). The future project known as Cherenkov Telescope Array (CTA), still under construction, will improve the IACT performance by expanding the energy range, improving the angular resolution and increasing the sensitivity by a factor 10 [9].

Gamma rays that reach the Earth's atmosphere interact with it, creating cascades of subatomic particles, known as air or particle showers. Light travels 0.03 % slower in air than in vacuum and as a result, these ultra-high energy particles can travel faster than light in air, producing a blue flash of Cherenkov light. Although the light is spread over a large area, the cascade only lasts a few billionths of a second. It is too faint to be detected by the human eye but not too faint for the Cherenkov Telescopes of IACT. The future CTA is a worldwide project which aims to build a new generation of ground-based gamma-ray detectors in the energy range covering from some tens of GeV until around 300 TeV. It is equipped with large mirrors and high-speed cameras which can detect the flash of light and image the cascade generated by the gamma rays for further study of their cosmic sources (see Figure 1.6) [10].

These cascades are unusual, with a rate of one gamma-ray photon per m^2 per year from a bright source or one per m^2 per century from a faint source. In order to detect them, CTA uses more than 100 telescopes spread between two array sites located in the northern and southern hemispheres to improve the possibility of detecting them [10]. These cascades cover a large area on the ground because they arrive very spread to the surface so they need to be observed at high altitude, typically around 2000 metres.

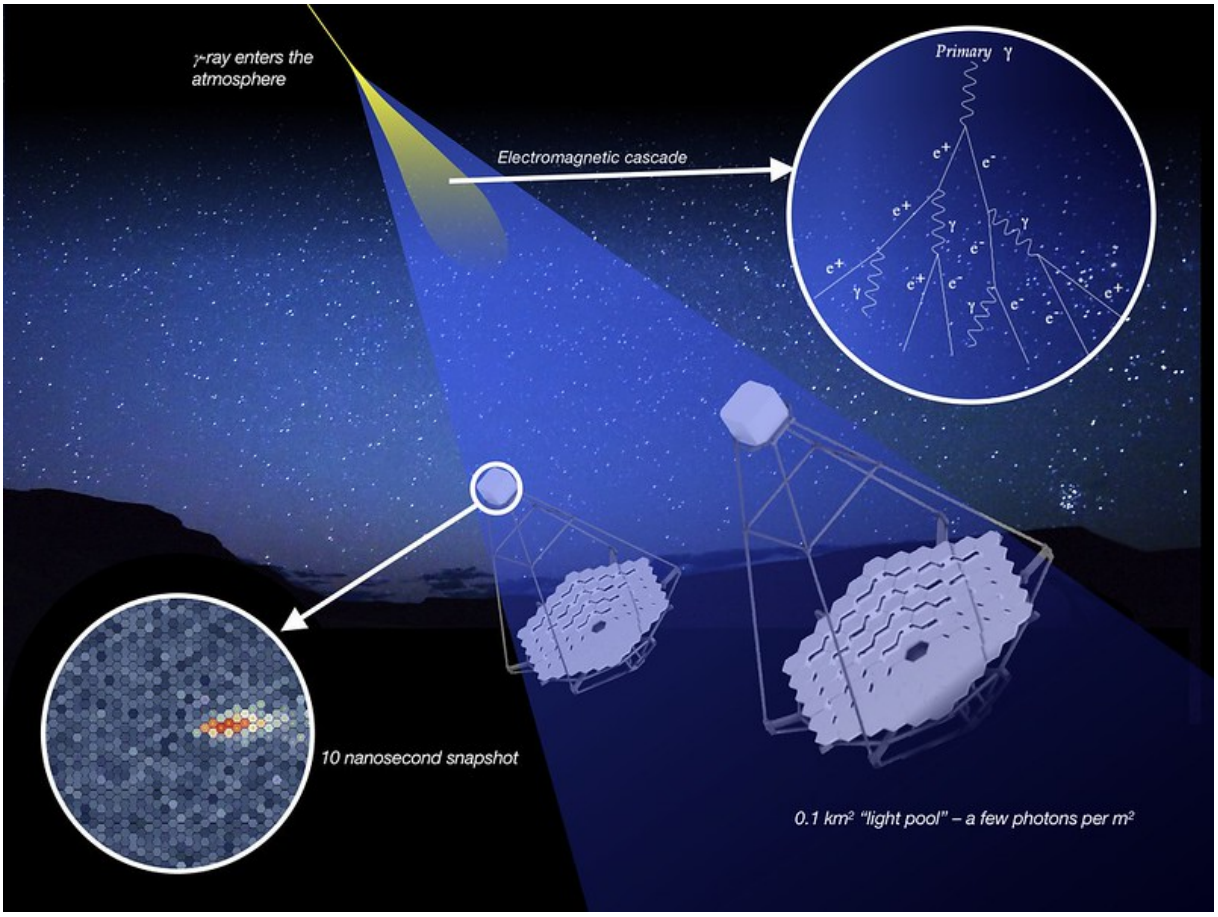

Figure 1.6: A schematic view of how a cascade and Cherenkov light is formed from a primary gamma photon and how the CTA mirrors will collect this light. Image taken from [11].

1.7. Overall pulsar properties

In this section, we will resume the main pulsar relations concerning its physical magnitudes. The most important property of a pulsar is its period P, since it can be measured very precisely, as well its rate of change $\dot{P}$ [2]. One of the main equations relates its characteristic age τ with its current and initial periods, P and P_0 respectively, summarised in Equation 1.1,

$$\tau = \frac{P}{(n-1)\dot{P}} \left[1 - \left(\frac{P_0}{P}. \right)^{n-1} \right] \tag{1.1}$$

being n the braking index, a parameter which describes the rate of loss of rotational energy. Experimental values of n lie in the range $2 < n < 3$.

Pulsar spin-down

The rate at which a pulsar loses rotational energy, $\dot{E} = \mathrm{d}E/\mathrm{d}t$, is compensated with a continuous injection of energy into the nebula from the pulsar. The majority of the

energy loss is due to radiation fields, and only a small fraction of it goes into the particles. Consequently $\dot{E}$ determines the energy injection history of a PWN [8]. Both magnitudes $\dot{E}$ and P decay at a similar rate according to:

$$\dot{E} = \dot{E}_0 \left(1 + \frac{t}{\tau_0}\right)^{-\frac{n+1}{n-1}} \qquad P = P_0 \left(1 + \frac{t}{\tau_0}\right)^{\frac{1}{n-1}} \tag{1.2}$$

where τ_0 is the initial spin-down timescale, and $\dot{E}_0$ is the initial spin-down luminosity. Typical values of τ_0 are around 10^3 years, while $\dot{E}_0$ values are 10^{40} erg s^{-1}. An important relation can be derived involving τ, τ_0, P and P_0 (see [8]).

$$\tau_0 = \frac{2\tau}{n-1}\left(\frac{P_0}{P}\right)^{n-1} \tag{1.3}$$

so the initial spin-down timescale can be inferred. Nevertheless, it must be mentioned that birth properties such as P_0, τ_0 or $\dot{E}_0$ are highly uncertain, since we measure current properties and try to figure out their initial values.

Radius evolution

Once the pulsar is formed in a SN explosion, the star and its PWN are surrounded by an expanding SNR. As described in Section 1.5 , at early times the pulsar is located near the SNR's center and the PWN expands rapidly. Assuming spherical symmetry the radius evolves as [12]:

$$R_{\text{PWN}} = 1.1 \left(\frac{\dot{E}_0}{10^{38}\ \text{erg s}^{-1}}\right)^{1/5} \left(\frac{t}{10^3\ \text{years}}\right)^{6/5} \quad \text{for } t < \tau_0. \tag{1.4}$$

Radius scales require to be measured in parsecs, an astronomic unit defined by the distance at which one Astronomical Unit (1 AU $\simeq 1.496 \cdot 10^{11}$ m) subtends an angle of one arc second, which is 1/3600 of a degree, 1". This gives us the relation 1 pc $\simeq 3.086 \cdot 10^{16}$ m. As the growth rate of a PWN depends on its stage, the radius time evolution goes through three phases, according to its initial spin-down timescale τ_0 and the RS interaction time, t_{rs}. The overall time evolution is [8]

$$R(t) \ \propto \ \begin{cases} t^{6/5} & \text{for } t \leq \tau_0 \\ t & \text{for } \tau_0 < t \leq t_{\text{rs}} \\ t^{3/10} & \text{for } t > t_{\text{rs}}. \end{cases} \tag{1.5}$$

Usually, the reverse shock occurs after τ_0, i.e $t_{\text{rs}} > \tau_0$. In the very uncommon case where the opposite occurs, the radius evolves as:

$$R(t) \ \propto \ \begin{cases} t^{6/5} & \text{for } t \leq t_{\text{rs}} \\ t^{11/15} & \text{for } t_{\text{rs}} < t \leq \tau_0 \\ t^{3/10} & \text{for } t > \tau_0. \end{cases} \tag{1.6}$$

In both cases, the proportionality constants can be derived applying continuity to $R(t)$ at τ_0 and t_{rs}, together with Equation 1.4 for first stage. Values of the reverse-shock time are

around 7 kyr and when this shock occurs, the PWN radius is drastically reduced, moving inwards, see Figure 1.5.

For much later times, this means for very old pulsars, we assumed radius evolved following electron diffusion, that is

$$R_d(t) \propto 2\sqrt{D \cdot \Delta t} \tag{1.7}$$

where D is the diffusion constant in our galaxy for 10 TeV electrons and Δt:

$$\Delta t = \begin{cases} t - t_{rs} & \text{for } t_{rs} < t \leq t_{cool} \\ t_{cool} - t_{rs} & \text{for } t \geq t_{cool}, \end{cases} \tag{1.8}$$

being t_{cool} the average cooling time for 10 TeV electrons.

Energy density

The energy density of a PWN is defined as energy contained in energetic particles within the PWN. It is estimated simply as

$$\varepsilon = \frac{E_{\text{inj}}}{V} = \frac{\dot{E}\tau}{V} \tag{1.9}$$

where V is the volume of the PWN and τ is the characteristic age of the pulsar. Here E_{inj} is the total energy injected in the PWN. Usually the energy density is shown in eV/cm^3 and studied at normalised energy densities, to check common behaviours or certain properties of them. Here we have used the pulsar properties as an approximation for the energy density, taking the pulsar $\dot{E}$ as a measure of power input, neglecting the energy losses.

Flux and luminosity

Flux and distances are magnitudes we can easily measure. In astronomy, usually luminosity (an intrinsic property of the source) is obtained measuring these two magnitudes and using Equation 1.10:

$$F = \frac{L}{4\pi d^2}. \tag{1.10}$$

Size

The angular size of a PWN in the sky can be obtained with simple trigonometry knowing the radius of the nebulae and the distance of a pulsar from

$$\text{Size} = \arctan\left(\frac{\text{Radius}}{\text{Distance}}\right), \tag{1.11}$$

where the radius evolution is obtained as described above and the angular size is measured in degrees.

Chapter 2

Objectives and Methodology

In this chapter, we will state the principal aims of this work, the assumptions made in our PWN model and the methodology followed throughout the project. Regarding the latter, we first discuss the data collection: from where the data was collected and why; how it was processed, treated and selected; and the procedure taken. We can distinguish two different parts, an initial generic study of the main pulsar properties and then a broader analysis of a larger sample in much detail. The analysis has been carried out in Python and the code has been entirely written on my own.

2.1. Objectives

At this moment there is a total number of 2547 pulsars detected in radio, according to the ATNF catalogue, explained further on. In contrast, there are only 40 PWNe detected in TeV energies, according to TeVCat, an online catalogue for TeV Astronomy [13]. This difference confirms the necessity of further research in higher energies detection, more precisely, in TeV energies. Therefore, the aim of this project is to search for pulsar candidates for future PWNe detections at TeV energies, since the majority of the pulsars have been detected in radio.

The work carried out can be summarised in a first study of the principal pulsar and PWN magnitudes, such as period, period rate, spin-down energy loss rate, age, energy density, flux, luminosity, among others. To accomplish it, we have worked with a reduced sample of young pulsars in the stage 1 described on Section 1.5, allowing us to validate the main pulsar properties and then to repeat some of our analysis performed here in other samples afterwards. Finally it also enabled us to establish some birth properties inferred from current measured quantities. Once the primary study has been performed, we have extended our sample, covering older pulsars and further PWN evolutionary stages. In this part of the study, we have focused again on the study of the energy density and, more in detail, we have studied the PWN flux-angular size relation with the HESS and CTA sensitivities. Finally, we have plotted the predicted TeV PWNe position and angular size along the Milky Way's galactic plane with its predicted relative surface brightness value for these TeV energies.

2.2. Assumed PWN model and constraints

In this section, we will describe the main assumptions of the applied PWN model. First of all, we assume a braking index $n = 3$, which is the value obtained for a pure magnetic dipole braking in vacuum whose derivation is available in detail in [14]. This choice is very common in the literature, shown in [12] or in [8] among others. This $n = 3$ debate around the braking index is discussed in many papers in the literature, for instance in [15]. Other approaches have been proposed, such as a non-dipolar field structure or a change in the magnetic inclination angle, but the magnetic dipole assumption, that is, $n = 3$, is the most accepted scenario currently. A pulsar's braking index can be estimated if the second derivative of the pulsar angular frequency can be measured, from $n = \Omega \cdot \ddot{\Omega}/\dot{\Omega}$ and experimental values obtained of n for some pulsars were lower. Few pulsars have known braking index due to the difficulty of measuring precisely $\ddot{\Omega}$, some of these n values can be found at [15]. For instance, for the Crab pulsar a braking index of $n = 2.51 \pm 0.001$ is estimated.

Using this assumption and assuming $P_0 \ll P$, which implies that the current period of the pulsar is much lower than the initial one (works better in older pulsars since period is constantly decreasing), Equation 1.1 turns into

$$\tau = \frac{P}{(n-1)\dot{P}}\left[1 - \left(\frac{P_0}{P}\right)^{n-1}\right] \qquad \longrightarrow \qquad \tau = \frac{P}{2\dot{P}} \tag{2.1}$$

which is a very well known relation for the age of a pulsar. An estimation of the typical lifetime values for pulsars can be inferred, around $10^5 - 10^8$ years. These derived lifetime values are overestimated probably due to the fact that experimental n values could imply pulsars are not a pure magnetic dipole. Giving a particular example, as stated in Section 1.1, for the Crab a value of $\tau = 1257$ years was obtained, despite having records of its explosion in 1054, which means a current age of 966 years. With $n = 3$, Equations 1.2 turn into

$$\dot{E} = \dot{E}_0 \left(1 + \frac{t}{\tau_0}\right)^{-2} \qquad P = P_0 \left(1 + \frac{t}{\tau_0}\right)^{-2} \tag{2.2}$$

and Equation 1.3 becomes

$$\tau_0 = \tau \left(\frac{P_0}{P}\right)^2 \tag{2.3}$$

We have also assumed an initial period $P_0 = 30$ ms for sake of simplicity. Since it is a birth property we cannot measure it directly, and any calculation of it will not be accurate, so this assumption can be done without a great loss of generality. Another assumption was the proportionality between the gamma-ray brightness and the energy density over square of the distance, ε/d^2, to obtain an energy estimation of each pulsar, briefly discussed the E_{inj} choice in Section 1.7.

With respect to the luminosity, here we have determined a relative gamma ray luminosity at 1 TeV for a generic PWN evolution, which can be appreciated in Figure 2.1, and

predictions for the flux have been made based on this model knowing luminosity and distance values in Equation 1.10. Consequently Figure 2.1 shows the luminosity interpolation normalised with respect to the Crab. Each pulsar's luminosity has been obtained multiplying the interpolation value by the $\dot{E}$ of the Crab.

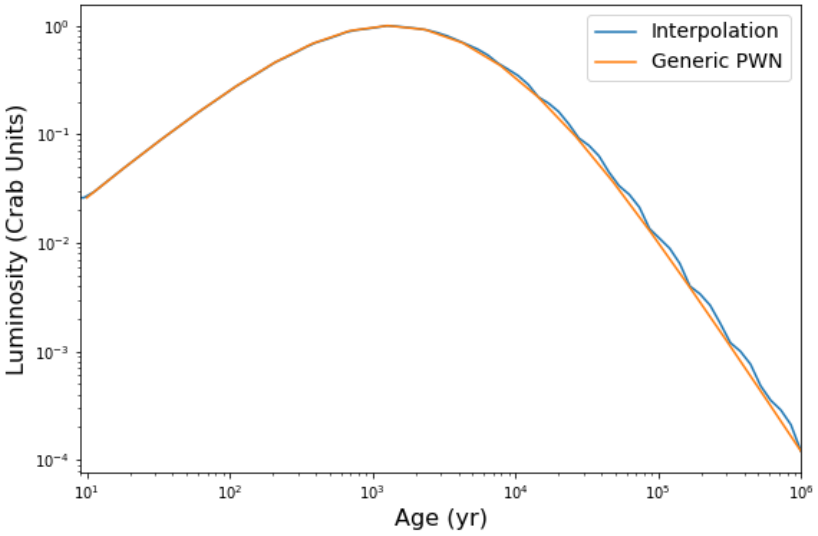

Figure 2.1: Generic PWN luminosity evolution with time. For each PWN age, a normalised luminosity value is obtained.

We have adapted the radius evolution stated in Section 1.7 following analytical studies of the development of PWNe in their SNR environment distinguishing the three expanding states and applying continuous boundary conditions (Equations 1.5 and 1.6). We have also assumed a free expansion phase as a fourth state, for much later times of the PWN, using diffusion theory as in Section 1.8, in contrast with the original version of the model in [16]. To delimit the different radius evolutionary stages we supposed the reverse shock occurs at $t_{rs} = 7$ kyr for all PWNe. Another assumption used in our model has been settling the cooling age for electrons at $t = 30$ kyr and chosing the diffusion constant in our galaxy for 10 TeV electrons as $D = 8.32 \cdot 10^{27}$ cm^2 s^{-1}. This value has been taken starting from [17] where the diffusion constant is $D = 8.32 \cdot 10^{28}$ cm^2 s^{-1}, but here reduced by a 10 factor due to the following assumptions: first the different electron energies lead to D approximately a factor 10 times larger due to the energy dependence of D. Second the experimental results (HAWC, geminga) suggest diffusion is approximately a factor 100 slower around pulsars than in the ISM. Both contributions gives us a diffusion constant $D = 8.32 \cdot 10^{28} \cdot 10/100$, so $D = 8.32 \cdot 10^{27}$ cm^2 s^{-1}. As mentioned in the radius evolution, spherical symmetry has been supposed for the PWN evolution.

In our model we have also defined the sensitivity as the minimal flux needed for a source, here pulsars, with the assumed spectrum in TeV to be detected above the background with a chosen significance 5σ. Taking into account that the PWN are extended sources, the total flux is distributed over a large area of the sky. Given a fixed background level,

the sensitivity of an instrument evolves as

$$F(\sigma_{\text{source}}) \propto \sqrt{\sigma^2_{\text{source}} + \sigma^2_{\text{PSF}}} \tag{2.4}$$

where σ_{source} is the size of the source and σ_{PSF} is the Point Spread Function of the instrument, a constant which depends on the detector, here we took cases for HESS and CTA detections, being 0.07 and 0.04 respectively. Equation 2.4 is constant for sources smaller than the PSF and increases linearly with source size for sources larger than the PSF. We also neglected statistical background uncertainties, although it can bias the sensitivity for very extended, large sources [18].

Finally, in order to identify halo candidates, we have taken as a first estimation that they have energy densities below 0.1 eV/cm^3. In [7], it is shown that the VHE gamma-ray emission from most TeV-bright PWNe is due to electrons and positrons contained in a region energetically influenced by the pulsar and therefore they do not constitute proper halos, where the TeV emission arises from a low energy density zone around the PWN. Clear unambiguous halo cases are those where the electrons responsible for the TeV gamma-ray emission propagate in a region where their contribution to the local total energy density is negligible, that is, energy densities below 0.1 eV/cm^3.

2.3. Collecting and processing data

2.3.1. Catalogues

CSIRO, Australia's national science agency, operates a number of world-class radio astronomy observatories, known as the Australia Telescope National Facility or ATNF. The ATNF is known as one of the world's most advanced astronomy facilities and it is the only one of its kind in the southern hemisphere. It offers a unique view of the southern hemisphere sky over a broad radio frequencies spectrum and occupies an important place in international radio astronomy. In addition, it is Australia's largest single astronomy institution and conducts 90 per cent of Australian radio astronomy research, covering subjects as evolution of galaxies, black holes or using pulsars to look for gravitational waves [19].

Entering into its results, the ATNF Pulsar Catalogue is a catalogue of known pulsars compiled by R.N. Manchester et al. and originally comes from the pulsar database used for the paper *Catalog of 558 Pulsars* available at [20], although it has been updated with published data from recent radio surveys. It is remarkable to compare the initial number of pulsars in the catalogue, 558, with the current one stated in Section 2.1, 2547, to understand the progress made in this field these last years. In particular, the catalogue includes all published rotation-powered pulsars and two small subsets of pulsars detected at high energies. The database table was at first created by the High Energy Astrophysics Science Archive Research Center, HEASARC [21].

2.3.2. Data processing

Once the ATNF catalogue has been introduced, we can at this moment enter into the approach taken to obtain and process the data object of this study. All pulsar samples have been taken from the ATNF Catalogue HEASARC Browser [21].

Sample 1

In order to check generic and common pulsar properties or connections between magnitudes, a preliminary study has been carried out. Here our aim is to become familiar with pulsars, their principal magnitudes and derive typical values for them. To do so our first sample, labelled Sample 1 hereafter, consisted on pulsars with period P greater than 10 ms and a spin-down luminosity $\dot{E}$ greater than 10^{35} erg s^{-1}. This P lower bound cut has been made to avoid milli-second pulsars in our sample, since they are old, low energy pulsars, different in terms of nature and physics of emission, considered a different population. They are usually members of binary systems that have gained matter from a secondary star, which provides an explanation for their short periods. Milli-second pulsars have much more stable pulsar periods and it can be inferred they have very weak magnetic fields and much greater ages. The other cut was related with the spin-down luminosity, where we have focused in young energetic pulsars, those with high $\dot{E}$ values. Both cuts enabled us to study $\dot{E}_0$ for different τ_0 values, which has been done rearranging Equation 2.2.

Sample 2

The intermediate study made has been based on the pulsar energy density and to accomplish it we introduced an age constraint, taking pulsars with age τ less than 7 kyr. We still avoided millisecond pulsars so we kept the $P > 10$ ms cut and slightly modified the $\dot{E}$ cut, becoming $\dot{E} > 5 \cdot 10^{32}$ erg s^{-1}, much softer constraint than before but enough to avoid very low spin-down luminosity pulsars. Summarising, our Sample 2 consists on young, not low energetic or millisecond pulsars still in their first evolutionary stage, when the reverse shock has not reached the PWN yet. There were only 26 pulsars with such constraint, meaning an age of 7 kyr is related with very young pulsars. However not all pulsars in the ATNF catalogue had a known distance, needed for our calculations, so the sample had been reduced until 21 pulsars.

A relative energy density study has been performed plotting ε/d^2 over $\dot{E}/d^2$ normalised with respect to the Crab, that is, by setting Crab values (J0534-2200) equal to 1 in both magnitudes. This allowed us to see connections between our pulsars and observe common behaviours of them towards, in this case, energy density and spin-down luminosity.

Sample 3

In order to carry out the main tasks of the project we took our large sample (Sample 3) of pulsars extending the age upper bound from 7 kyr until 500 kyr but without modifying

P and $\dot{E}$ constraints of Sample 2. It resulted in 304 pulsars object to study, more than ten times the size of the previous sample of young pulsars. Since there are many old pulsars in this sample, some assumptions such as the radius evolution following electron diffusion were taken for very old times. Compared to the 7 kyr sample, some calculations were repeated, including the energy density study with respect to the Crab, in relative units, or the initial period study. Magnitudes such as angular size or flux were obtained, carrying out a study relating the flux relative to the Crab and angular size predicted, together with CTA and HESS sensitivities. From this study a list of candidate pulsars for future TeV detections can be determined. We have also determined pulsars with angular size greater than 2 degrees and simultaneously pulsars with flux greater than the Crab. Another study towards identifying possible halo candidates has been carried out, following assumptions made in our PWN model. Finally, a map in galactic coordinates (see Section 2.3.3) of our pulsar sample has been made emphasising the relative surface brightness magnitude with a coloured scale map of each predicted PWN at TeV energies.

The data processing has been performed using Python. The developed code for each Sample is open access in GitHub under this repository.

	$\dot{E}$ (erg s^{-1})	P (s)	τ (kyr)
Sample 1	$> 10^{35}$	> 0.01	-
Sample 2	$> 5 \cdot 10^{32}$	> 0.01	< 7
Sample 3	$> 5 \cdot 10^{32}$	> 0.01	< 500

Table 2.1: Cuts in pulsars spin-down luminosity, period and age for each sample.

2.3.3. Galactic Reference Frames

Apart from the Equatorial Coordinate system, using Right Ascension (RA) and Declination (Dec), the Galactic Coordinate System is used too. It is a celestial coordinate system, with the Sun in its center in spherical coordinates, the primary direction aligned approximately with the center of the Milky Way galaxy and the equator of the system along the galactic plane.

Its coordinates are the galactic longitude l and the galactic latitude b, measured in degrees. The first one measures the angular distance of an object from the center towards the east, while b measures the angle of an object towards the north. The angular size of the PWN can be measured by the angle with which it is seen from the Earth, which is measured in degrees and have values $\lesssim 5°$, since it is difficult to measure angular sizes greater than 5°.

2.3.4. Pulsar Nomenclature

Astronomical objects show real movements such as orbital and proper motions, varying over the years. The epoch is a moment in time used as a reference point for some time-varying astronomical quantity, like celestial coordinates. It defines the date for which the position of an object applies.

There have been usually two systems, B1950 (old one) and J2000, the current one. For example, the pulsar formed in the Crab Nebula SNR is called PSR J0534+2200 (in J2000), but is known as PSR B0531+21 too, where PSR stands for Pulsar Source Radio. However, pulsars are often referred to by their discovery name, so B1950 is generally used for earlier discoveries. The name J0534+2200 stands for the Right Ascension, as Crab's RA is 05 34 (hh mm), and Declination which is +22 00 in (dd mm) for Crab. Notice RA is measured in hours while Dec in degrees. As it is appreciated, hours, minutes and seconds are used to locate pulsars using these coordinates, discussed in Section 2.3.3. The 360°is split into 24 hours, which are split again into 60 minutes (') and each minute into 60 seconds (").

The current standard equinox and epoch used, J2000.0, means January 1, 2000 at 12:00 TT and the prefix J indicates a Julian epoch. Instead, in B1950, for the previous epoch (from 1950), the prefix B means it was a Besselian epoch. As in the Crab example, a pulsar may be refered to with both of each nomenclature, having at the same time a B and a J names if the pulsar was discovered before the J2000 came into use.

Consequently pulsars recently discovered do not have a B name and pulsars discovered before 1993 usually retain their B names rather than their J name. The pulsar prefix, for example PSR, means how the pulsar has been discovered, in this case in radio (Pulsating Source of Radio). Other prefixes used for PWN are TeV, HESS, HWC among others.

Chapter 3

Results and Conclusions

In this chapter, we will show results for our samples and the conclusions drawn. This chapter can be divided in two sections, the first part deals with Samples 1 and 2 (described in Section 2.3.2) and their conclusions about some common pulsar properties and preliminary studies. The second part resumes the large Sample 3 and the main results of the project, concerning the predicted candidates for TeV detections the halo population estimation and a PWN map in galactic coordinates with the estimated surface brightness at TeV and angular sizes.

3.1. Preliminary study

$\dot{P}$–P and $\dot{E}$–τ diagrams

Starting with our Sample 1, with cuts $P > 10$ ms $\dot{E} > 10^{35}$ erg s^{-1}, the $\dot{P}$–P and $\dot{E}$–τ diagrams can be appreciated in Figure 3.1. Unless specified, we will talk about pulsars in Sample 1. Starting with $\dot{P}$–P diagram located at the left part of Figure 3.1, it enables us to relate the main property of pulsar, its very precise spin period P, with the spin-down rate at which the pulsar slows down, $\dot{P}$, both independently measured. This diagram is useful for following the life of pulsars, playing a similar role to the Hertzsprung–Russell diagram for ordinary stars. Plotting lines of constant values can give a tremendous amount of information about the pulsar population and its properties in terms of P and $\dot{P}$. Here we have plotted three different lines for characteristic age τ, current spin-down luminosity $\dot{E}$ and minimum magnetic field strength B. Following this order, constant characteristic age lines can be obtained from Equation 2.1.

$$\tau = \frac{P}{2\dot{P}} \longrightarrow \dot{P} = \left(\frac{1}{2\tau}\right) \cdot P \tag{3.1}$$

Moving to constant lines for spin-down luminosity, $\dot{E}$ the following equation must be rearranged as:

$$\dot{E} = -\frac{4\pi^2 I \dot{P}}{P^3} \longrightarrow \dot{P} = \left(-\frac{\dot{E}}{4\pi^2 I}\right) \cdot P^3 \tag{3.2}$$

and finally for magnetic field lines, we know the minimum magnetic field strength at a surface for a canonical pulsar is [6]:

$$\left(\frac{B}{\text{gauss}}\right) > 3.2 \cdot 10^{19} \cdot \left(\frac{P\dot{P}}{\text{s}}\right) \longrightarrow \dot{P} < \left(\frac{B}{3.2 \cdot 10^{19}}\right) \cdot \frac{1}{P} \tag{3.3}$$

Only a lower bound can be established, since to estimate the exact field we must know the angle α between both magnetic and rotation axis. In fact, this inequality comes from applying the sine function is bounded, in this case $\sin\alpha < 1$. As a reminder, we said in Section 1.3 that both axis must be misaligned, so $\sin\alpha$ must be strictly between 0 and 1. Referring to the $\dot{E}$–τ plot located at the right part of Figure 3.1, similar constant lines can be plotted, in this case related to constant total remaining energy $\dot{E}\tau$ in the pulsar, according to

$$\dot{E} = \dot{E}_0 \left(\frac{\tau}{\tau_0}\right)^{-2} \tag{3.4}$$

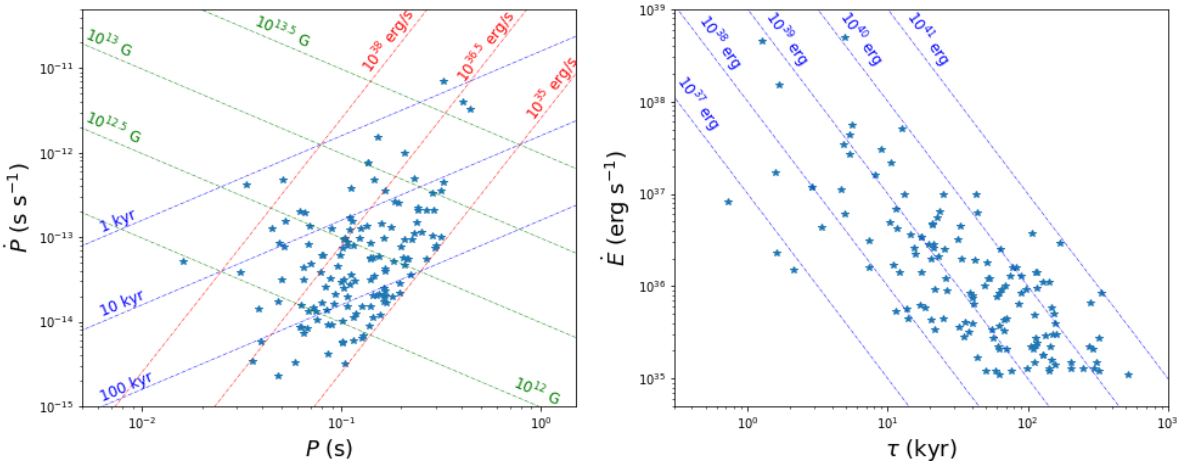

Figure 3.1: *Left:* Plot of the independent measures quantities P and $\dot{P}$ of our Sample 1. Lines show constant values of spin-down luminosity $\dot{E}$ (in red), minimum magnetic field strength B (green) and characteristic age τ (blue). The $\dot{E} > 10^{35}$ erg s^{-1} cut can be appreciated in the lower part of the plot where many pulsars have spin-down luminosities close to the bound. *Right:* $\dot{E}$–τ plot for our Sample 1. Constant remaining energy lines are also shown following the approach of [8]. Both plots appear in logarithmic scale.

Once both diagrams have been introduced, the main conclusion we can obtain is that, $\dot{P}$–P plot shows a great percentage of pulsars present ages between 10-100 kyr, corresponding to their second evolutionary stage and therefore not old pulsars, since the constraint on the spin-down luminosity assured our sample consisted on energetic young pulsars. This idea is observed in the $\dot{E}$ straight lines, where all pulsars lie over the 10^{35} erg s^{-1} line as expected and we can estimate typical values of the spin-down luminosity are between $10^{35} < \dot{E} < 10^{38}$ erg s^{-1}, for young, energetic pulsars. With respect to the minimum magnetic field, magnetic field strengths are greater than 10^{12}–10^{13} gauss, extremely high values. To add some context, the average field on the surface of the Earth is around 0.5

gauss and in the Sun an average field of 1 gauss.

The $\dot{E} > 10^{35}$ erg s^{-1} cut can be appreciated in the $\dot{E}$–τ diagram, as mentioned in Figure 3.1 caption, and strengthens the same conclusion inferred from the constant $\dot{E}$ lines shown in $\dot{P}$–P plot. Total remaining energy constant lines shows typical values of energy a pulsar release, very high quantities. They lie between 10^{43} and 10^{47} erg and, as we have stated in Section 1.7 a pulsar releases a total amount of energy around 10^{49}–10^{50} erg over its whole lifetime, so these young but energetic pulsars have a small fraction of energy remained, less than a 1% of their initial energy.

$\dot{E}$ and τ_0 study

Working with our Sample 1 of young, energetic pulsars, we now focus on inferring typical values of the initial spin-down luminosity. As it is said, it is a birth property and therefore it is not measured directly, in contrast to $\dot{E}$, P or $\dot{P}$. Therefore $\dot{E}_0$ can only be estimated. At the same time we have studied the initial spin-down timescale τ_0 taking usual values. In our model we explicitly mentioned $\tau_0 = 10^3$ years, which will be taken further on, but here close τ_0 values have been taken.

$\dot{E}_0$ has been studied for different values of τ_0 for this sample to observe how this distribution evolved. In order to do so, we chose the following values of τ_0 which were $10^{2.5}, 10^{2.75}, 10^3, 10^{3.25}$ and $10^{3.5}$ years. However, only histograms for the extreme values, $10^{2.5}$ and $10^{3.5}$ yr are shown in Figure 3.2, where the magnitude studied was $\log_{10} \dot{E}_0$, that is, the exponent when expressed in base 10. We can observe the differences of both distributions. The $\dot{E}_0$ distribution for $\tau_0 = 10^{2.5}$ years lie mainly between 10^{40} and 10^{41} erg s^{-1} while the shift is appreciated for $\tau_0 = 10^{3.5}$ descending until 10^{38} and 10^{39} erg s^{-1}. This behaviour, that we obtain greater values of $\dot{E}_0$ when taking small values of τ_0, can be previously predicted from Equation 2.2 from the dependency of τ_0 and $\dot{E}_0$.

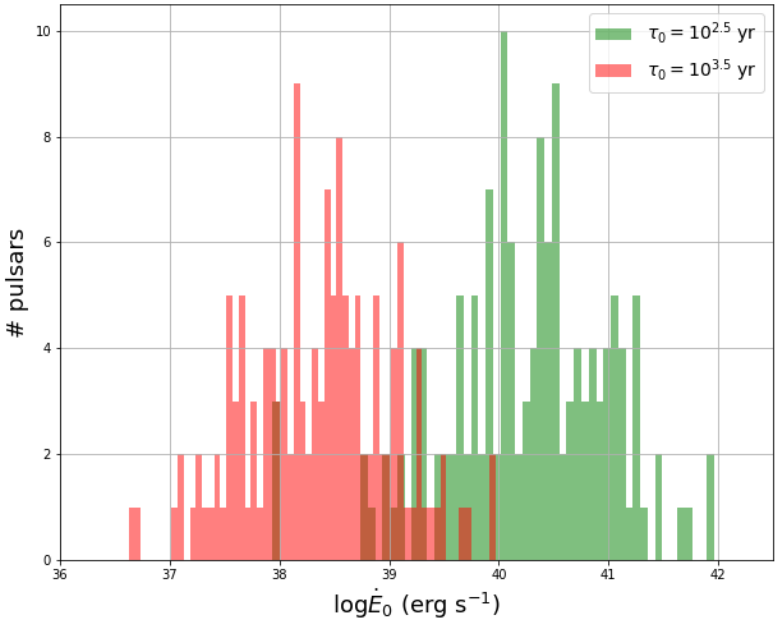

Figure 3.2: $\dot{E}_0$ distributions for the least and the greatest τ_0 values for our Sample 1 of energetic pulsars. While the greatest τ_0 distribution lie around $\log_{10} \dot{E}_0 = 38.4$, the smallest one is around $\log_{10} \dot{E}_0 = 40.5$.

The study made for all five τ_0 different values can be appreciated in Figure 3.3, where the Gaussian distributions have been plotted to study how $\dot{E}_0$ evolves for typical values of τ_0. As before, we have centered in $\log_{10} \dot{E}_0$ and apart from the descendent behaviour, we notice the smaller τ_0, the less centered the gaussian is, being more spread. Mean μ and standard deviation σ of these normal distributions are qualitatively resumed in Table 3.1. While the standard deviation does not drastically change, the mean is clearly shifted towards smaller values. Again μ and σ here refer to logarithm values, so for the typical choice $\tau_0 = 10^3$ years, the results are $\dot{E}_0 \simeq 10^{39.3} \pm 10^{0.7}$ erg s^{-1}. Same notation applies for all τ_0 values: the mean is 10^{μ} erg s^{-1} and the standard deviation is 10^{σ} erg s^{-1}.

τ_0 (yr)	μ	σ
$10^{2.5}$	40.23854	0.75759
$10^{2.75}$	39.75242	0.74299
10^{3}	39.27504	0.72165
$10^{3.25}$	38.81072	0.69284
$10^{3.5}$	38.36504	0.65748

Table 3.1: Values of mean (μ) and standard deviation (σ) of each distribution for different values of τ_0.

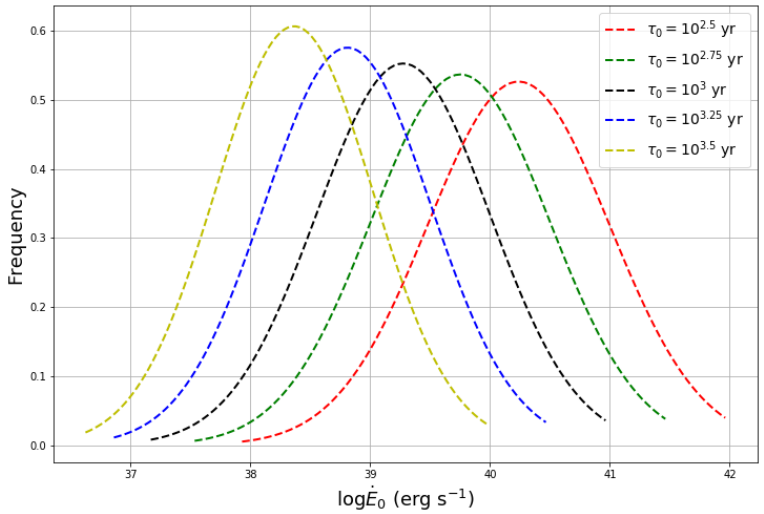

Figure 3.3: Gaussian distributions of $\dot{E}_0$ for different values of τ_0. We observe qualitatively there is no change a great change in the standard deviation but with respect to the mean distribution, there is a shift to the left as τ_0 values increase. Mean variation in percentage along τ_0 values range from 1.21 % in the first shift (yellow to blue curves) descending up to 1.15 % in the last one (green to red).

Sample 2 study

At this stage we focused on our Sample 2 of pulsars younger than 7 kyr to carry out an initial study of their energy density. With constant value $P_0 = 30$ ms, we have obtained τ_0 and $\dot{E}_0$ with Equations 2.2 and 2.3, being τ_0 average around 1236 yr, close to the common assumption $\tau_0 = 10^3$ yr. Concerning $\dot{E}_0$, values range from 10^{38} erg s^{-1} to 10^{44} erg s^{-1}, being on average closer to this last value. We need both magnitudes to obtain the radius from Equations 1.4, 1.5 or 1.6, depending on their PWN radius evolutionary stages and once with this magnitude, each spherical volume could be calculated. Then the energy density can be obtained from Equation 1.9.

This section has been studied with respect to the Crab, so unless specified, magnitudes and conclusions will be in Crab terms, arbitrary units for our model.

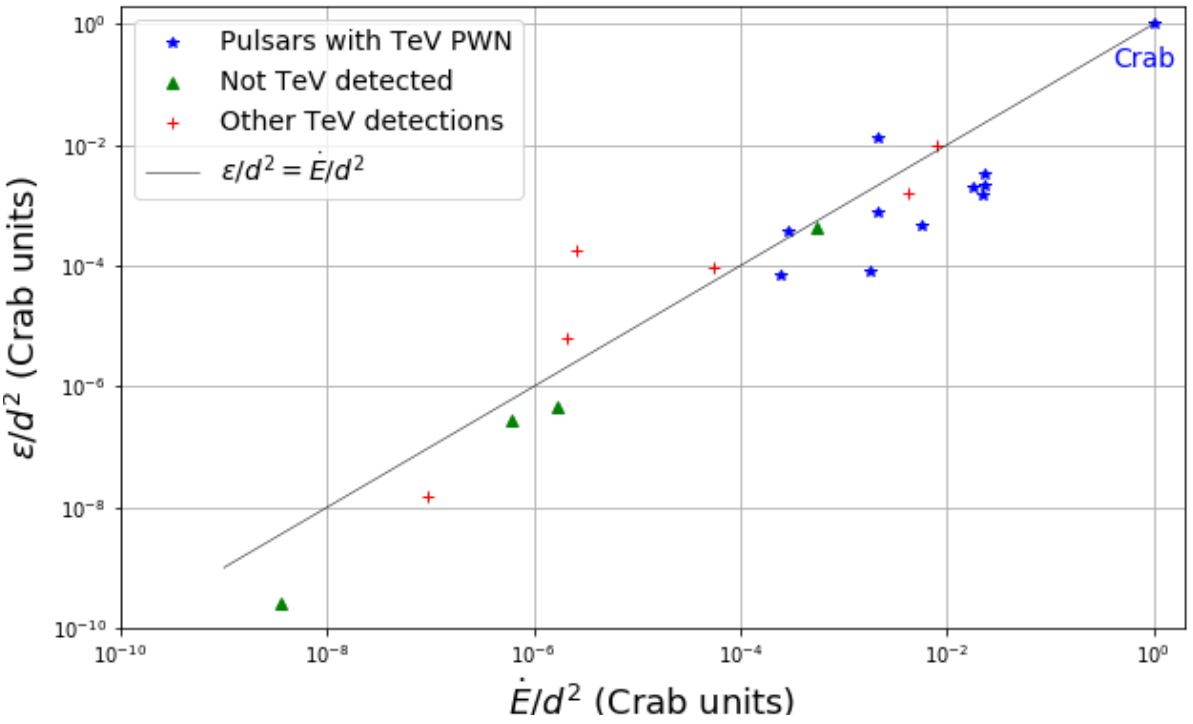

Figure 3.4: Energy density over distance square against $\dot{E}$ over distance square. Magnitudes have been normalised to the Crab and since it was the highest value in both magnitudes, it is located at point (1,1). Three different types of pulsars have been distinguished. Highest ε/d^2 pulsar not TeV detected is J0540-6919.

It should be recalled that our Sample 2 consists on pulsars younger than 7 kyr, a very strong age constraint so we do not expect a great number of pulsars to study yet. Having said this, the sample can be divided into three groups of pulsars, according to whether or not associated PWNe have been detected in the pulsar at TeV energies. As resumed in the legend of Figure 3.4, blue dots are pulsars which have a PWNe already detected and confirmed. Red dots correspond to pulsars with overlapping TeV emission that has not been firmly identified as PWN yet and finally green dots are pulsars without PWNe detected at TeV energies. This classification has been made according to TeVCat 2.0 Catalogue [23] and the three different classes of pulsars defined above have been studied too, consisting of 11, 6 and 4 pulsars in each subgroup, respectively. Finally, the straight line $\varepsilon/d^2 = \dot{E}/d^2$ in Crab units has been plotted to qualitatively analyse its relation based on the Crab. Pulsars with PWN firmly identified are shown in Table 3.2 with its base 10 logarithm Crab coordinates and both HESS and ATNF names.

As previously explained, all logarithm values are negative meaning all ε/d^2 are smaller than one, consequently smaller than the Crab. A total of 11 pulsars out of 21 are located in this group, more than half of our sample, all lying in the upper right part of the plot corresponding to high ε/d^2 and $\dot{E}/d^2$ values, which is reasonable as there is more likelihood in those pulsars to be detected due to their higher density and spin-down luminosity

with respect to the distance.

$\dot{E}/d^2$ is an excellent PWN detection estimator, since it relates the spin-down luminosity and distance, two important variables when measuring PWNe, and in general celestial objects. For example, a PWN with high $\dot{E}$ located at a very large distance will have a smaller $\dot{E}/d^2$ value than a closer one with similar $\dot{E}$. Same comparison applies with a close but faint PWN and a more distant with higher $\dot{E}$ one.

Name HESS	Name ATNF	$\log_{10} \varepsilon/d^2$ (Crab)	$\log_{10} \dot{E}/d^2$ (Crab)
Crab	J0534+2200	0.000	0.000
J1846-029	J1846-0258	−1.8877	−2.6695
J1023-575	J1023-5746	−2.4973	−1.6459
3C58	J0205+6449	−2.6770	−1.6301
J1833-105	J1833-1034	−2.7173	−1.7452
J1813-178	J1813-1749	−2.8259	−1.6472
J1930+188	J1930+1852	−3.1063	−2.6622
G0.9+0.1	J1747-2809	−3.3243	−2.2389
J1119-614	J1119-6127	−3.4387	−3.5380
J0537-691	J0537-6910	−4.0843	−2.7537
J1640-462	J1640-4631	−4.1689	−3.6187

Table 3.2: Pulsars with PWN firmly identified at TeV with their ε/d^2 and $\dot{E}/d^2$ value in base 10 logarithm normalised to the Crab, ordered by decreasing ε/d^2. Both HESS and ATNF names are shown, but it can be observed how ATNF names follow the J2000.0 epoch, showing the pulsar RA and DEC in hours and minutes (hhmm), while HESS names are sometimes shown with less precision in their declination, appearing only three digits instead of four. Some of the names are related with their first discovery, for instance in G0.9+0.1, G stands for 'Green's SNR catalogue', followed by its galactic coordinates l and b.

Table 3.3 shows pulsars with TeV detections not yet strongly identified together with their current classification. Before entering into further detail of Table 3.3, it must be remarked that what it is confused and not clearly established is the identification with TeV emission. That is, relating the TeV emission with its source, since pulsar association with extended TeV emission is usually confused. Different classifications can be observed, starting from composites, when the PWN is surrounded by a SNR and we cannot tell them apart, a very common classification until the object is distinguished. The SGR G327.1-1.1 is coincident with a Soft Gamma-ray Repeater (SGR) partially identified as a magnetar, another type of neutron star with even more powerful magnetic fields than pulsars. In this case, due to HESS J1808-204 being coincident with both the SNR and SGR, the source is still considered unidentified (UNID). Finally the pulsar J1713-3810 is apparently associated with the shell-type SNR CTB 37B. Pulsar J1841–0456 could be confused with HESS J1841-055, which is likely to be associated with the pulsar formed at SNR Kes 73. However this TeV source has also been proposed to be connected with PSR J1838–0537. These kind of proposals are very common in the literature when two

or more pulsars have similar coordinates and their identification with TeV emission is usually confused.

Name	ATNF Name	Classification
J1514-591	J1513-5908	Composite
SNR G292.2-0.5	J1124-5916	Composite / PWN
J1841–055	J1841-0456	Composite / SNR Kes 73
J1808-204	J1808-2024	UNID (SGR 1806-20)
SNR G327.1-1.1	J1550-5418	Composite / PWN
CTB 37B	J1714-3810	Shell SNR

Table 3.3: Pulsars with overlapping TeV emission but not firmly identified. Their current classification is shown too. Some of them are considered as composites since we cannot tell apart the PWN and SNR, while J1808-2024 is still unidentified (UNID) but with a candidate and finally J1714-3810 is considered a shell of a SNR.

The third group of pulsars not yet TeV detected is the smallest one, with only four of them. From greatest ε/d^2 to least shown in Table 3.4. J1745-2900 is a pulsar located in the Galactic Centre, the rotational center of the Milky Way galaxy and formed by a supermassive black hole (SMBH). Its coordinates in the equatorial coordinate system are: RA 17h 45m 40s and Dec $-29°00'$ 28.1", very similar to the pulsar coordinates, so the proximity to the SMBH could be the reason of not detecting it in TeV energies, although it must be mentioned the Galactic Centre is a very confused region. J0100-7211 pulsar is located far away at the Small Magellanic Cloud so here the main reason could be the too high distance. Similarly, the pulsar J0540-6919 is in the Large Magellanic Cloud (LMC),both the SMC and LMC are satellite galaxies of the Milky Way with a high negative declination nearly -70°. Clearly these sources are extragalactic as they are outside the Milky Way. In addition J0540-6919 is also the first extragalactic gamma-ray pulsar discovered. The last pulsar J1050-5953 is still undetected in these energies, could be owing to insufficient time observations.

ATNF Name	Reason for no detection
J0540-6919	LMC - Extragalactic
J1745-2900	Galactic Centre
J1050-5953	Undetected
J0100-7211	SMC - Extragalactic

Table 3.4: Pulsars without TeV emission detected together with the main reason of why each of them have not been detected yet. LMC/SMC stand for Large/Small Magellanic Cloud. They have been listed from greater to lower ε/d^2 values relative to the Crab.

3.2. Sample 3 analysis

In this section, we present the main results of this work, which are related with Sample 3, the last, large sample of pulsars. Mainly three studies has been made, concerning the energy density and flux, a halo population estimation and a galactic coordinates map of the estimated surface brightness at TeV and angular sizes with the aim of predicting future PWN TeV detections.

3.2.1. Energy density study

The first study is related to the energy density and based on the study made in Section 3.1 for our young pulsars Sample 2. A similar energy density study has been made to more deeply examine the dependence of the energy density with the spin-down luminosity, over distance square for a much broader number of pulsars. In addition, we are able to compare these results with those of Figure 3.4 which was carried out for young pulsars and then infer how the relation between the variables ε/d^2 and $\dot{E}/d^2$ evolves in both young and old pulsars cases relative to the Crab.

One of the main differences with respect to the previous study was adding the last stage of the radius evolution governed by Equation 1.7, used to obtain estimations for each PWN spherical volume to them obtain the energy density ε with Equation 1.9. As previously, our task was to plot ε/d^2 against $\dot{E}/d^2$, again normalised to the Crab, which had the greatest ε/d^2 and $\dot{E}/d^2$ values. This meant so our data was once more contained in the unit square with the Crab in the upper right corner, emphasising once more the importance of the Crab PWN in this study and, in general, in the PWN field. The ε/d^2 Crab value was $1.3 \cdot 10^{-3}$ eV cm^{-3} pc^{-2}, while $\dot{E}/d^2$ for the Crab was $1.125 \cdot 10^{32}$ erg s^{-1} pc^{-2}. With these values and the normalised plot, initial ε/d^2 and $\dot{E}/d^2$ could be arranged for each pulsar too. The energy density plot is shown in Figure 3.5.

We have divided our results according to two different classifications: whether they were on the previous sample (that is, pulsars younger than 7 kyr) and whether they had TeV PWN firmly associated, this latter division similar to the one made in the previous energy density study. As one of the objectives of this plot, we can compare the young pulsars represented with circles with the rest described with crosses. It is interesting to study the relation between both magnitudes with the plot of straight lines whose slopes enable us to infer that relation. Therefore we added the following three straight lines:

$$\frac{\varepsilon/d^2}{\dot{E}/d^2} = 1 \qquad \frac{\varepsilon/d^2}{\dot{E}/d^2} = 0.1 \qquad \frac{\varepsilon/d^2}{\dot{E}/d^2} = 0.01 \tag{3.5}$$

where colours match with their graphic representation. As concluded in the Sample 2 study in Figure 3.4, the majority of young pulsars lied around the straight line $\varepsilon/d^2 = \dot{E}/d^2$, in comparison with the whole large Sample 3 where there is a huge portion of them lying between the blue and red lines. It means young pulsars (from Sample 2) are more energetic than old ones. Therefore TeV discovered pulsars have similar energy density and spin-down luminosity while the rest of pulsars older than 7 kyr are located between the

blue and red lines, that is, with their energy density between 10 and 100 times lower than their spin-down luminosity. It is straightforward to observe that pulsars older than 7 kyr pulsars are below the black line, meaning $\varepsilon/d^2 < \dot{E}/d^2$. This much lower energy density comes from the fact that older pulsars have their PWN much spread in the ISM. Although the spin-down luminosity has decreased too, energy density has done at a greater pace due, in part, to the cubic dependence on the PWN radius. Moreover, pulsars have already entered into stage 2 or even stage 3 in their PWN evolution discussed in Section 1.5. It should be recalled magnitudes are in Crab units, meaning all conclusions and comments are with respect to Crab ε/d^2 and $\dot{E}/d^2$, used as a reference.

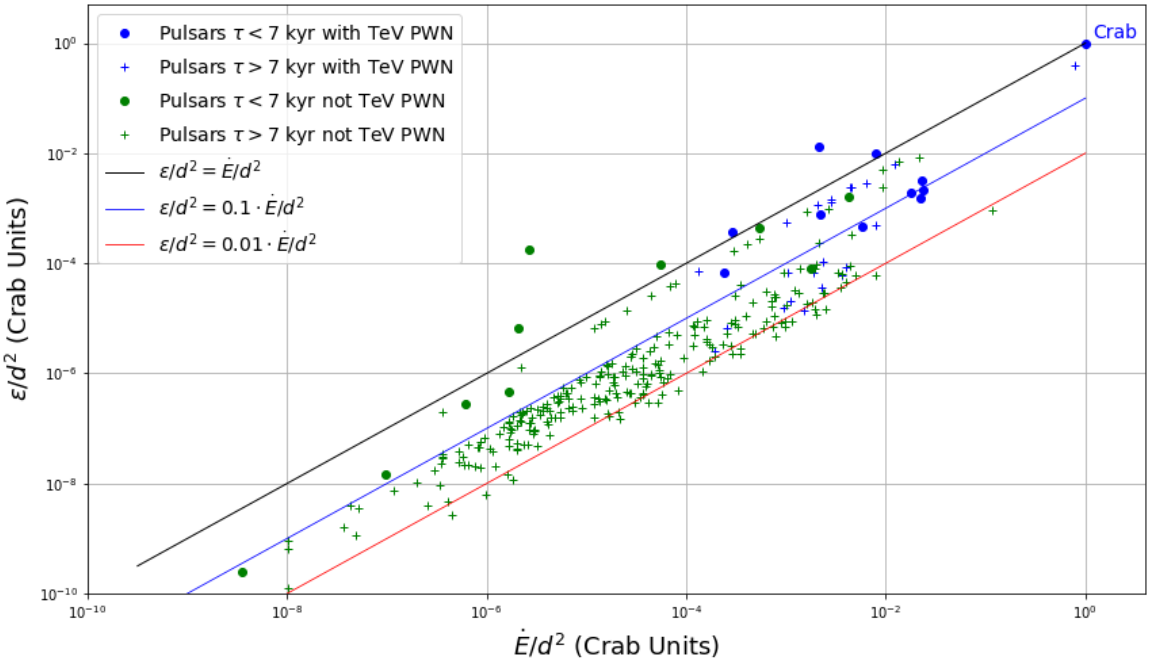

Figure 3.5: Plot of ε/d^2 against $\dot{E}/d^2$, normalised to the Crab value, which is the blue dot at (1,1). Discovered TeV pulsars and young pulsars have been distinguished. Straight lines to show different quotients between the plotted variables are shown too.

3.2.2. Flux-angular size study

At this point, we have focused on the flux of PWNe and angular size of their associated PWNe in the sky. Hereafter, size refers to angular size. As in the energy density study, the last radius evolutionary stage based on diffusion theory had been added. In contrast with the general astronomy procedure where flux and distance of a source are measured and then luminosity is inferred, here we first obtained each pulsar's normalised luminosity with respect to the Crab following the model based on the interpolation curve of Figure 2.1. Labelling our interpolation as $\mathcal{I}$, then a pulsar luminosity has been obtained from

$$L = \mathcal{I}(\tau) \cdot \dot{E}_{\rm cr} \tag{3.6}$$

where τ is the age of that pulsar, $\mathcal{I}(\tau)$ the interpolated luminosity of that pulsar and $\dot{E}_{\rm cr}$ is the spin-down luminosity of the Crab pulsar. Therefore the flux of each PWN can be obtained from Equation 1.10 and the known variables luminosity and distance. They were mainly inside the interval $10^{26} < F < 10^{31}$ and the average flux was around 10^{30} erg s^{-1} pc^{-2}. Once more we normalised it to the Crab flux, which was $8.93 \cdot 10^{30}$ erg s^{-1} pc^{-2}. Despite it was a high value in our sample, this time it was not the greatest value, unlike in the energy density study. This leads to a few amount of pulsars which had fluxes greater than the unit, once normalised to the Crab. Only there were three of them, shown in Table 3.5 with their main pulsar properties: spin-down luminosity, distance and characteristic age. We have shown $\log_{10} \dot{E}$ instead of $\dot{E}$. These three pulsars are very close to us, at a distance less than 1 kpc, since this distance is considered nearby, within astronomy. It could be the reason of their large flux.

Name (ATNF)	Flux (Crab Units)	Size (°)	$\log_{10} \dot{E}$ (erg s^{-1})	d (pc)	τ (kyr)
J0940-5428	1.474	6.24	36.28	380	42.2
J1740-3015	3.919	2.28	36.84	280	11.3
J0835-4510	16.357	1.40	34.91	400	20.6

Table 3.5: Pulsars with greater predicted PWN flux than the Crab Nebula. We show their names, together with PWN predicted size and relative predicted flux, as well as common properties such as the spin-down luminosity (in base 10 logarithm), distance and characteristic age.

With respect to the size of the nebula in the sky, we have obtained it from Equation 1.11, using once more the radius evolutionary stages from Section 1.7. Typical values are no more than a few degrees and normally, less than a degree. This is due to the large distances at which pulsars are usually located (a few kiloparsecs), which makes them appear very small from the Earth.
Therefore a great size could be due to either a large nebula or a pulsar located nearby. Most of our PWN had sizes smaller than a degree, another portion between one and two degrees and only 18 pulsars, out of 304, had sizes greater than two degrees. These pulsars have been studied in Table 3.6 in a similar way as Table 3.5. Although here we are dealing with angular sizes, it must not be forgotten PWNe with the same physical sizes can have different angular sizes due to their distance, according to Equation 1.11.

All 18 pulsars, except one, have $d \leq 1$ kpc, meaning the ratio radius/distance is large, and consequently, the size. We can then point out the small distance as one of the reasons of a large PWN size. We have highlighted this subsample because in our flux vs size plot we have limited it to PWN with sizes less than 2°, so pulsars in Table 3.6 will not appear there.

Name (ATNF)	Size (°)	$\log_{10} \dot{E}$ (erg s^{-1})	d (pc)	τ (kyr)
J0922+0638	2.136	33.83	1100	497
J1740-3015	2.279	34.91	400	20.6
J0908-4913	2.362	35.69	1000	112
J1020-5921	2.499	32.92	940	485
J1809-2332	2.678	35.63	880	67.6
J2337+6151	3.357	34.80	700	40.6
J1732-3131	3.682	35.18	640	111
J0924-5302	4.611	33.53	510	333
J0954-5430	5.466	34.20	430	171
J0942-5657	5.739	33.48	410	323
J0940-5428	6.240	36.28	380	42.2
J1003-4747	6.362	34.48	370	220
J1001-5507	7.849	32.83	300	443
J1825-0935	7.854	33.66	300	232
J1741-2054	7.855	33.98	300	386
J0942-5552	7.855	33.49	300	461
J0659+1414	8.127	34.58	290	111
J0633+1746	12.46	34.51	190	342

Table 3.6: PWN with size greater than 2° shown in a similar way as Table 3.5.

Figure 3.6 resumes this flux-size study. Following the same idea from the energy density study we have distinguished between pulsars with PWN TeV detected and not firmly TeV detected. Flux has been plotted in Crab percentage, rather than Crab units. Back to Table 3.5, we observe only one pulsar out of the three pulsars with greater predicted flux than Crab appears. Two of the three pulsars have angular sizes greater than 2°and do not appear. The only pulsar from Table 3.5 appearing, with a predicted flux value of 1635.716 (% Crab), more than 16 times Crab flux value, is J0835-4510, also named Vela. This Vela pulsar has been, together with the Crab pulsar, of special importance because they were young pulsars with ages consistent with the ages of the SNR. Among all pulsars, a small portion of them (33 out of 304) were TeV detected, appearing as blue dots in the plot and displayed in Table 3.7. Geminga appears in this table, since its size is $\simeq 12.46°$. This huge value of size comes from being too close to us in comparison to the rest, as it has been discussed in Section 1.1 too.

The two curves appearing stand for CTA & HESS sensitivity and scale with the size of the source according to the relation described in Equation 2.4 taking σ_{PSF} 0.07 for HESS and 0.04 for CTA. We have assumed a sensitivity of 1% Crab for HESS, following a similar idea as described in [18] and for CTA we have assumed a sensitivity of 0.1% Crab. A vertical line at 0.7° has been made to compare this plot with the one in [18], as well as current and future sentivitites of the facilities.

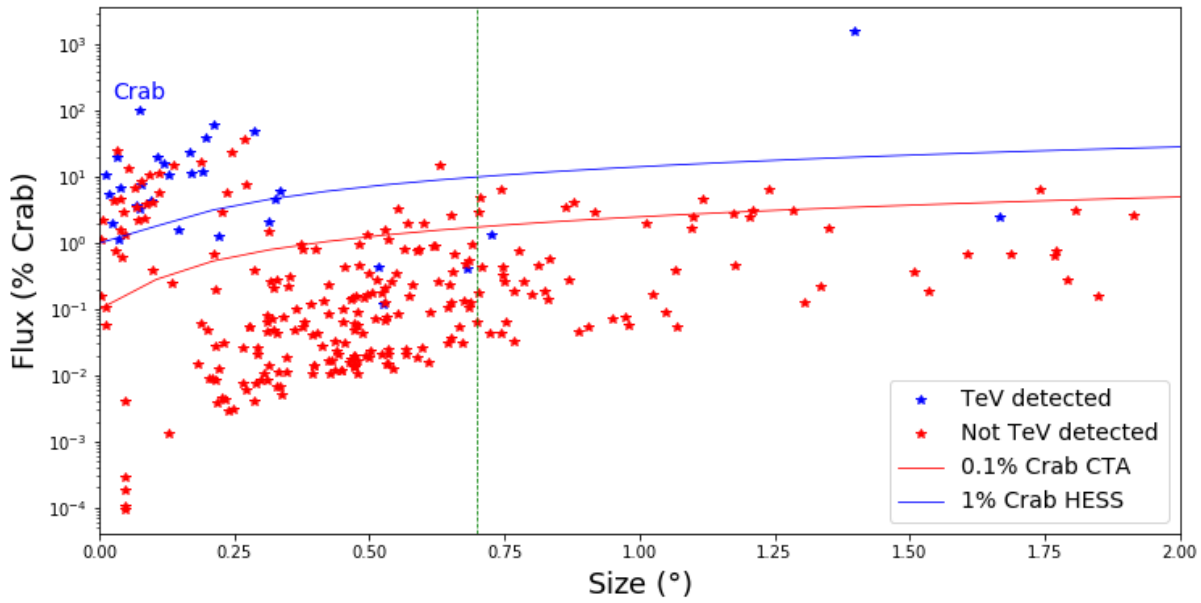

Figure 3.6: Source flux vs PWN size scatter plot identifying pulsars with PWN firmly detected (blue) and pulsars not firmly PWN detected at TeV, in red. To obtain a better resolution plot, we did not show PWN whose size was greater than 2°, which were a total of 18. Sensitivity curves for HESS (1% Crab) and CTA (0.1% Crab) have been illustrated too. A vertical line at 0.7° has been added corresponding to the limit of the HGPS [18].

Pulsars with TeV PWN detected of Figure 3.6 have been listed in Table 3.7, being a total of 33 pulsars, approximately a 10 % of our sample. However two of these pulsars have sizes greater than 2°and consequently they do not appear. They are J0659+1414 and J0633+1746, the latter one also know as Geminga. It is suprising how these pulsars with great angular sizes have been TeV detected, but it is because these two pulsars have extended gamma-ray detected. It has been recently reported in [24] that using the High Altitude Water Cherenkov Observatory (HAWC) extended TeV gamma-ray emission has been detected at locations coincident with J0633+1746 (Geminga) and PSR B0656+14, which is another designation for J0659+1414.

Name	Name	Name
J1357-6429	J1301-6305	J1119-6127
J1418-6058	J1420-6048	J1513-5908
J1016-5857	J1028-5819	J1023-5746
J1617-5055	J1640-4631	J0835-4510
J1709-4429	J1718-3825	J1747-2809
J1803-2137	J1811-1925	J1809-1917
J1813-1749	J1826-1334	J1833-1034
J1857+0143	J1838-0655	J1846-0258
J1857+0143	J1856+0245	J1907+0602
J0659+1414	J0633+1746	J1930+1852
J0534+2200	J0205+6449	J0007+7303

Table 3.7: ATNF name of pulsars TeV detected. Two of them shown in red have sizes greater than 2°and are beyond the size limits.

Having a look at those pulsars above the HESS curve, a total of 28 pulsars out of 50 pulsars have not been firmly identified yet. As they are above both curves, these ones become in probably future candidates for being detected and established. These candidates appear in Table 3.8.

This study of pulsars identified can be compared to the study carried out in [18]. There, 31 out of 78 pulsars were firmly identified (39%), while in this study only 33 out of 304 (11%).

Name (ATNF)	$\log_{10} \dot{E}$ (erg s^{-1})	d (pc)	τ (kyr)
J1708-4008	32.76	3800	8.90
J1841-0456	33.00	9600	4.57
J0501+4516	33.08	2200	15.7
J1050-5953	33.75	9000	2.68
J1745-2900	34.11	8300	3.40
J1726-3530	34.54	4720	14.5
J1714-3810	34.61	13200	1.03
J1746-2850	34.62	5610	12.7
J1632-4818	34.68	5310	19.8
J1808-2024	34.70	13000	0.218
J1734-3333	34.75	4460	8.13
J1740-3015	34.91	400	20.6
J1550-5418	35.00	4000	1.41
J1958+2846	35.53	1950	21.7
J1856+0113	35.63	3300	20.3
J1907+0631	35.72	3400	11.3
J1413-6141	35.75	8490	13.6
J1702-4310	35.80	4320	17.0
J1614-5048	36.20	5150	7.42
J0940-5428	36.28	380	42.2
J1048-5832	36.30	2900	20.3
J1801-2451	36.41	3800	15.5
J2021+3651	36.53	1800	17.2
J1826-1256	36.56	1550	14.4
J1124-5916	37.08	5000	2.85
J2229+6114	37.34	3000	10.5
J2022+3842	37.48	10000	8.94
J1400-6325	37.71	7000	12.7

Table 3.8: Future pulsars candidates for PWN TeV detection, lying above both HESS and CTA sensitivity curves, ordered from lowest to greatest $\dot{E}$. They are shown with their main magnitudes: base 10 logarithm of $\dot{E}$, distance and characteristic age.

3.2.3. Possible halo sources

In this section, we have studied the energy density of our sample as a function of $\dot{E}$ and τ, separately, to look for new TeV halo candidates. We have already introduced halo sources in Sections 1.5 and 2.2, considered to have energy density below 0.1 eV/cm^3. Both plots are summarised in Figure 3.7 and, focusing on those possible candidates for halo sources, we have obtained the mean of the age and $\dot{E}$ for this set of pulsars. The average age was 218.17 kyr, whilst average $\dot{E}$ was 7.4248 $\cdot 10^{34}$ erg s^{-1}.

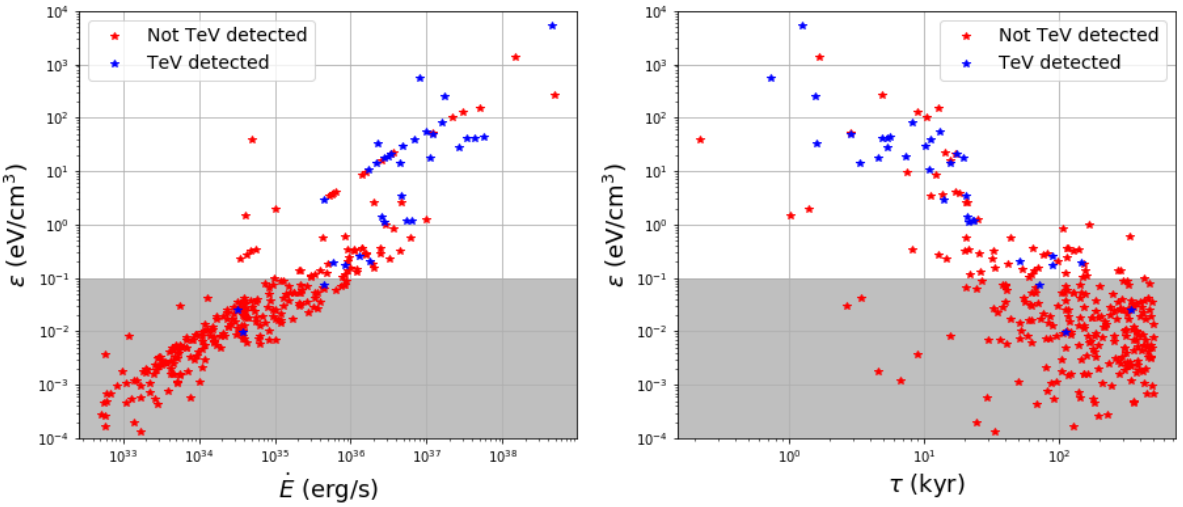

Figure 3.7: Left: energy density against $\dot{E}$. Right: energy density against τ. In both cases, the shaded regions correspond to an energy density lower than that of the ISM under any reasonable assumption.

215 pulsars have possible halos, which represents almost a 71 % of the whole sample. The three pulsars with TeV PWN firmly detected are shown in Table 3.9 with their plotted magnitudes. There is one pulsar, J1857+0143, which is on the edge of being classified as halo, and still unclear if the TeV emission is really associated with this pulsar. This is supported by the fact its predicted halo energy density is the highest of these three pulsars and can be appreciated it is very close to the $\varepsilon = 0.1$ eV/cm^3 limit.

Name (ATNF)	$\log_{10} \dot{E}$ (erg s^{-1})	ε (eV/cm^3)	τ (kyr)
J1857+0143	$4.5 \cdot 10^{35}$	71	0.0735
J0659+1414	$3.8 \cdot 10^{34}$	111	0.0098
J0633+1746	$3.2 \cdot 10^{34}$	342	0.0254

Table 3.9: Pulsars with TeV emission detected which have possible halos with their magnitudes $\dot{E}$, ε and τ, showed in Figure 3.7.

3.2.4. Predicted PWNe in the Milky Way's galactic plane

Finally, using galactic coordinates, i.e. galactic longitude and latitude, (l, b), together with angular size values, in degrees, and surface brightness, a map of the predicted PWNe has been obtained restricted to latitudes $b < |5|$ degrees. To take the angular size dependency into account we have introduced the surface brightness, defined as flux per unit solid angle, that is, per unit angular area on the sky. For a PWN, surface brightness is its flux over its area, taken as $4\pi R^2$. Surface brightness enables us to study and relate flux and size of PWNe, since flux itself is not a good estimator and needs to be related with distance with surface brightness.

The whole map was divided into three submaps, to divide the (0,360) limits of longitude and to improve the visibility of the small size PWNe. Therefore, each PWN appears in the map as a circle centered in the (l, b) coordinates of the pulsar and radius its PWN size. In addition, a coloured map was made, showing the relative surface brightness of our sample, meaning a PWN with low flux (relative for our sample) will appear with a dark, red colour, whilst a PWN with large flux (again, compared with our sample) will have a brighter, orange/yellow colour.

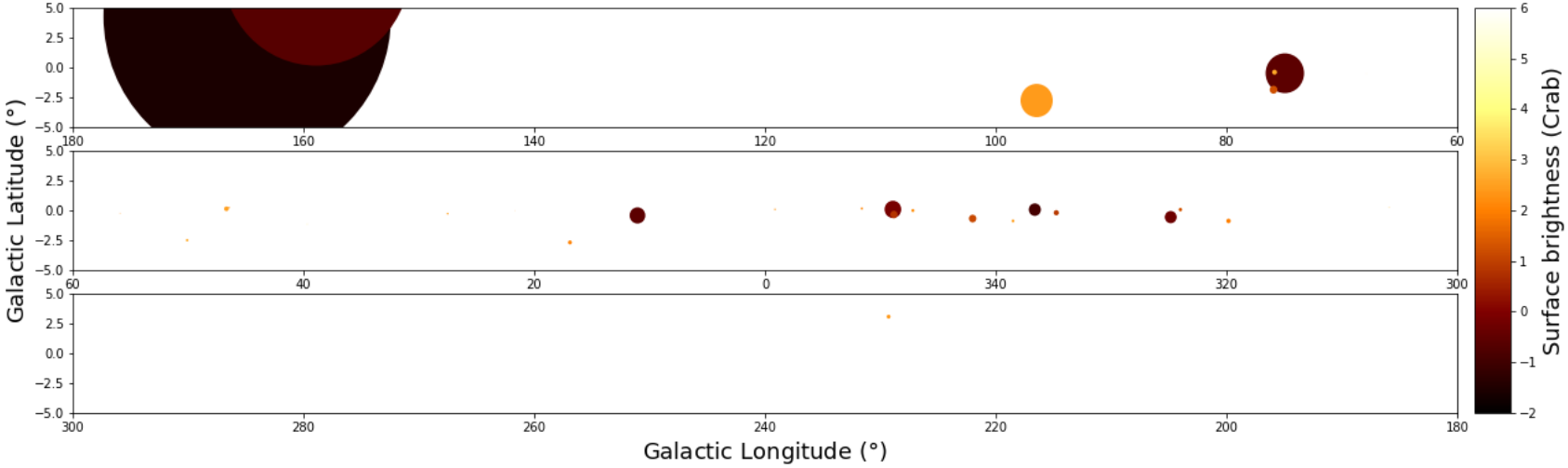

Figure 3.8: Predicted PWNe in the Milky Way galactic plane in galactic coordinates for pulsars with PWN firmly identified at TeV, divided into three subplots and restricted to galactic latitude values $b < |5|°$.

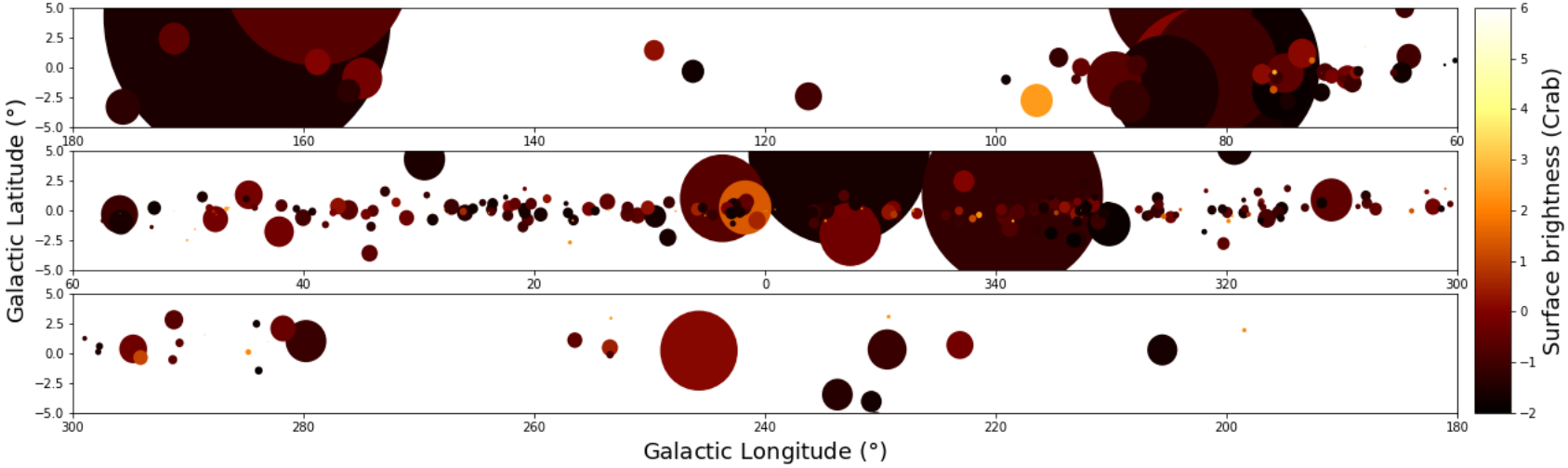

Figure 3.9: Predicted PWNe in the Milky Way galactic in galactic coordinates for all Sample 3 pulsars, divided into three subplots and restricted to galactic latitude values $b < |5|^{\circ}$.

Chapter 4

Discussion and further work

4.1. Discussion

First of all, we must highlight the way we have approached the study, starting with two "test" samples (Sample 1 and 2) based on energetic pulsars and young pulsars, respectively. After drawing common conclusions about pulsars magnitudes and behaviour, we were able to broaden our work, knowing in advance the behaviour of energetic and young pulsars. We could then study the behaviour of older pulsars in Sample 3 and compare it with the acquired knowledge for Samples 1 and 2, as it can be exemplified in the two energy density studies presented in Sections 3.1 and 3.2.

Our first main result has been the initial $\dot{P}$–P and $\dot{E}$–τ diagrams for Sample 1, where we have been able to study and relate pulsar magnitudes such as period, period derivative, spin-down luminosity, characteristic age or remaining energy. But these diagrams also give us information about the type of pulsars we are dealing with. Therefore we can compare our diagrams with the general pulsar $\dot{P}$–P and $\dot{E}$–τ diagrams, that is, with no constraints on any magnitude, to have an overall view of these relations and where the energetic, young pulsars lie on the $\dot{P}$–P plot, since it is immediately seen in the $\dot{E}$–τ plot. Figure 4.1 shows the general plot made for a large unconstrained 1000 pulsar sample. Two different regions can be appreciated in both plots. In the $\dot{P}$–P plot there is a small region of pulsars with periods between 1 ms and 10 ms whose period rate $\dot{P}$ does not substantially vary, being this rate around 10^{-20} s s^{-1} and therefore much lower in comparison with the rest. This set of pulsars lying in the lower left part of the plot corresponds to millisecond pulsars, a type of pulsars we have avoided throughout our work. Briefly introduced in Section 2.3.2, we stated that they are considered as a different population of pulsars due to their nature. We also stated they had very stable pulse periods, proved by the fact $\dot{P}$ is much lower. Looking at $\dot{E}$–τ diagram, we observe how $\dot{E}$ evolves along pulsar's lifetime described by τ, as expect the spin-down luminosity decreases with time.Again, the millisecond pulsars can be easily differentiated due to their low period rates which result in being very old pulsars from the relation $\tau = P/(2\dot{P})$. Their old ages have already been briefly mentioned in Section 2.3.2, but it is graphically supported by Figure 4.1. This specific behaviour justifies the reason of excluding them from our sample as their properties are much different than the rest of pulsars.

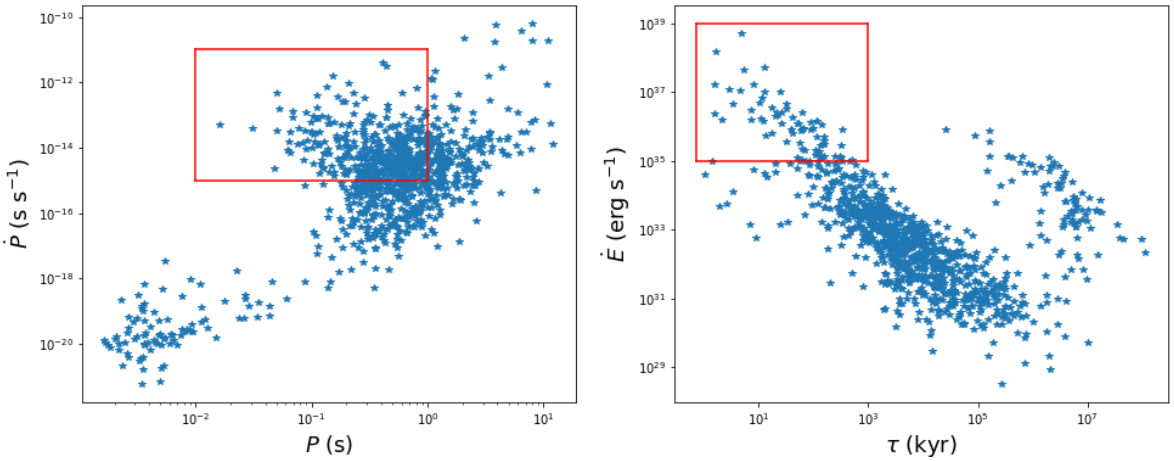

Figure 4.1: $\dot{P}$–P and $\dot{E}$–τ diagrams showing the complete known pulsar population with no constraints. A red rectangle showing the region plotted in Figure 3.1 has been made to compare both general diagrams.

Centering on the energy density plots in Figures 3.4 and 3.5, we have seen typical locations for ε/d^2 and $\dot{E}/d^2$ depending on whether a pulsar has TeV PWN associated or not, for instance pulsars with TeV PWN detections are located below but close to the black straight line $\varepsilon/d^2 = \dot{E}/d^2$ relative to the Crab.

Also it is interesting to perform a deeper study for our small Sample 2 of young pulsars and analyse each pulsar individually, focusing on the young pulsars with confused TeV detection, that is, where there is TeV emission detected but its identification is not firmly identified. With a small group of six pulsars resumed in Table 3.3, we have compared the different types of sources before being firmly established, such as composites, magnetars, SNR shells or even the common case of a region where there is TeV emission detected but it has not been identified with any object yet, in this case known as UNID. Similar study for pulsars with no TeV detections has been carried out but in contrast with the previous study here we could not classify them and instead we gave a plausible reason for not being detected in TeV energies yet, mainly based in their location, such as being in the Galactic Centre or in the SMC and LMC. In astronomy one of the main reasons for not properly identifying a source is due to the insufficient observation time for the current facilities, here exemplified with J1050-5953. CTA aims to solve this observational constraint for a large number of objects.

However, this deep study cannot be adapted for Sample 3, due to the large number of pulsars here, roughly 300. Although we were not able to draw the same conclusions, we were able to compare both samples regarding ε/d^2 and $\dot{E}/d^2$ behaviour with respect to the Crab. Figure 3.5 shows that pulsars became less efficient than Crab with time, it means, as while pulsars evolves with time, their volume increase and their energy output decreases, but their efficiency is very low in comparison with the Crab, between 10 % and 1 % for the majority of the pulsars added in Sample 3. This low efficiency comes from the fact that as pulsars evolve with time, their energy output decreases and the PWN

volume increases, but the energy density decreases at a greater pace than the energy. Energy dependence of the variables can prove some justification on this low efficiency. Equation 2.2 shows $\dot{E} \propto t^{-2}$, while radius dependence varies depending on the different PWN stages, described in Section 1.7. Taking as an approximation $R \propto t$ for sake of simplicity, and since $V \propto R^3$, we arrive at $\dot{E}/R^3 \propto t^{-2}t^{-3}$, which is not independent of time. Therefore, in the majority of pulsars the energy density is lower than the spin-down luminosity, $\varepsilon/\varepsilon_{crab} < \dot{E}/\dot{E}_{crab}$ (with respect to the Crab).
However, we observe some TeV detected pulsars lie around the blue straight line, corresponding to $\varepsilon/d^2 = 0.1 \cdot (\dot{E}/d^2)$. This means 10 % efficiency with respect to Crab, which can shed some light on future studies of energy in pulsars or towards predicting future detections based on their energy density relative to the Crab. Pulsars located above the blue line of Figure 3.5 could be detected in TeV energies in the future with CTA project.

Focusing on the flux-size plot in Figure 3.6, according to the predicted PWN flux we have listed a group of candidate pulsars for future TeV detections with CTA. CTA aims to improve HESS sensitivity up to 10 times, and to give an idea of its impact, if current detectors have increased the number of known gamma-ray-emitting objects approximately from the order of 10 to 100, CTA will expand the catalogue over ten times, aiming to detect more than 1000 new objects. This list of future candidates is resumed in Table 3.8, one of the main results of this work. Space and time limitations did not allow us to make a further study on these 18 pulsars, a similar one to the one made in Tables 3.2, 3.3 and 3.4 but adapted and modified to this plot, by checking each pulsar individually both in the TeVCat catalogue and in the literature. The vertical line of Figure 3.6 is plotted to compare the flux-size study carried out in [18] studying the HGPS flux sensitivity limit. A small comparison has been made in Section 3.2 about the percent of pulsars identified with TeV emission. The HGPS was not sensitive to larger angular sizes, up to approximately 0.7°, but in the future CTA should be sensitive to angular sizes up to 2 degrees.

Regarding the halo study, we have shown that there is a great percentage of pulsars that can have possible halos, but as mentioned in Sections 1.4 and 1.5, halos can only exist in advanced PWN evolutionary stages, usually from the stage 2 on. We have followed a similar study as in [7]. Figure 3.7 shows that there are many pulsars close to the established energy density $\varepsilon = 0.1$ eV/cm^3 limit, on the edge of being classified as possible halo sources. It shows the halo classification is still ambiguous and to be further studied.

Finally, the map of candidates of PWN to be detected in galactic coordinates for the subsample of PWN TeV detected and the whole Sample 3 shown in Figures 3.8 and 3.9 respectively, aims to predict the future PWNe population in TeV energies, which will be carried out by CTA telescopes and facilities. Since the majority of pulsars have small galactic latitudes, $|b| < 5°$, we have taken this restriction. The majority of sources do not have a great surface brightness relative to the Crab as expected, but some bright sources appear. Figure 3.9 can give an idea of the difficulties in measuring these sources in the TeV sky, since in many occasions they cannot be distinguished, or they are confused with each other or merely they are not bright enough, as there are lots of faint sources, again with respect to the Crab.

The entire project also points out the importance in the field of the Crab pulsar and Crab Nebula, since this work has been made taking Crab as a reference in practically all studies but the initial diagrams: energy density, flux-size and the galactic coordinates map centered on the galactic plane with surface brightness relative to the Crab. To justify this relative study, we must note in astronomy is very common to chose a reference object and express magnitudes relative to that object. In stars it usual to encounter masses, luminosities or radii in Sun units: $M_\odot$, $L_\odot$ or $R_\odot$, or even defining a unit as the distance between the Sun and the Earth, 1 AU. In a similar way in pulsars the Crab is taken as reference.

Additionally, we have made a first approximation study about the contribution of PWNe to Cosmic Rays (CR) to see whether PWNe could be responsible for a fraction of CR. We took the energetic pulsars of Sample 1 and obtained the energy density due to pulsars in the Milky Way (MW) from Equation 1.9 taking MW's volume $V_{\text{MW}} = 6.65 \cdot 10^{66}$ cm^3. We obtained $\varepsilon_{\text{MW}} = 0.000123$ eV/cm^3, much lower than the CR energy density, 1 eV/cm^3 according to [25]. This means PWNe does not largely contribute to CR. The fact we have only taken the most energetic pulsars and not all pulsars does not modify since low energetic pulsars do not contribute in a great way.

4.2. Further work

Lastly, we will describe further paths towards a possible future continuation of the project. We have briefly mentioned in the discussion the possible division of Figure 3.5 between TeV detections not firmly identified and pulsars not TeV detected, although it could be very time consuming and tedious to check each pulsar individually. Alternatively, there is not a great number of pulsars with $\varepsilon/\varepsilon_{crab} > 0.1\dot{E}/\dot{E}_{crab}$, which are those above the blue line of 3.5, so a similar study could be done to that subsample. Following the same process, the threshold can be lowered to enlarge the TeV detections not firmly identified, depending on how big our new subsample becomes, since the closer to the line $\varepsilon/\varepsilon_{crab} = \dot{E}/\dot{E}_{crab}$, the more probable to be TeV detected.

Another possible option is to modify some of the assumed values in our PWN model described in Section 2.2 such as the reverse shock time, where we have used 7 kyr. Instead, we can establish different reverse shock values in function of the current pulsar stage or even define a Gaussian distribution for t_{rs} centered at the used value 7 kyr and using known pulsar values for a better approach to obtain t_{rs}. Another Gaussian distribution can be either applied for the radius values in order to modify the strong spherical assumption and not obtaining perfect circles in Figures 3.8 and 3.9. Examining the t_{rs} in depth, we have said it occurs at different times for each PWN, but also for different directions in the same PWN. In Figure 1.5 this anisotropy can be appreciated, where the reverse shock reaches the PWN before in some directions than others. Another assumed value was the diffusion constant, but in fact it depends on the energy, meaning the radius of the very old PWNe will show an energy dependence not considered here. Similar idea applies for the cooling age of electrons, taken constant as 30 kyr.

With respect to the birth properties, here in the Sample 3 study we have chosen $\tau_0 = 10^3$ yr and $P_0 = 30$ ms for all pulsars. Different modifications can be carried out to observe how energy density or radius evolves. Although here we have not taken $\dot{E}_0$ as free parameter and instead we have obtained it from both birth magnitudes τ_0 and P_0, the process can be swapped.

The flux-size plot in Fig 3.6 can be improved regarding the HESS and CTA curves by adding a width bar representing a gaussian distribution to obtain a further study of HESS and CTA sensitivities, as in [18], or going into further research of our list of candidate pulsars of Table 3.8 as made in the energy density study for Sample 2 in Tables 3.3 and 3.4.

For our galactic maps, on the one hand, we could change surface brightness profiles so that a PWN is brighter in the center of the PWN, corresponding to the pulsar location, and that it becomes less bright towards the edge. On the other hand, we have obtained a total of 143 sources overlapping, that is, 143 sources that appear in Figure 3.9 overlapped with another one. It means it will not be easy for CTA to firmly detect them. To distinguish two sources, they must not have similar coordinates (l, b) and neither similar radius or brightness. Therefore we can define a threshold quantity to distinguish two separate sources, for example a minimum difference in brightness (relative to the Crab) between two PWNe, or a minimum separation between their galactic (l, b) coordinates in order to resolve them. If we relate this modification with the previous idea of making surface brightness brighter at the centre and fainter towards the edge, the threshold brightness could allow us to distinguish more sources since the brightness takes the PWN radius into account.

To conclude, as a remark we must remind that we have performed this study for a gamma-ray energy of 1 TeV. Similar studies can be repeated for different energies either lower like 100 GeV or greater such as 10 TeV or 100 TeV. Some aspects of the model may vary, like the gamma ray luminosity, the cooling age for electrons or the diffusion constant, specially observed in older systems. Taking this study as a reference, we should obtain a greater population for lower energies as 100 GeV and a smaller population for greater energies.

Bibliography

[1] Hewish et al. *Observation of a Rapidly Pulsating Radio Source*, 1968. Nature Vol 217, 10.1038/217709a0. Available at: https://www.researchgate.net/publication/32005350_Observation_of_a_Rapidly_Pulsating_Radio_Source.

[2] Malcolm S. Longair, *High Energy Astrophysics*, Third Edition, University of Cambridge. Pages 406-410.

[3] Chandra X-ray Observatory website. *Stellar evolution photo*, from: https://chandra.si.edu/graphics/xray_sources/stellar_fate.jpg.

[4] AstroPix website. *Crab Nebula from Five Observatories*, from: https://astropix.ipac.caltech.edu/image/spitzer/ssc2017-05a1.

[5] Pulsar & Neutron Stars, Formation of Neutron stars and Pulsars. Source: http://web2.uwindsor.ca/courses/physics/high_schools/2013/Pulsars/pulsars02.html.

[6] National Radio Astronomy Observatory website, *Essential Radio Astronomy*, Pulsars. Available at: https://www.cv.nrao.edu/~sransom/web/Ch6.html

[7] G. Giacinti, A. M. W. Mitchell et. al, *On the TeV Halo Fraction in gamma-ray bright Pulsar Wind Nebulae*. Available at https://www.aanda.org/articles/aa/abs/2020/04/aa36505-19/aa36505-19.html.

[8] H.E.S.S. Collaboration, *The population of TeV pulsar wind nebulae in the H.E.S.S. Galactic Plane Survey*, Astronomy & Astrophysics **612** A2 (2018). Available at: https://www.aanda.org/articles/aa/full_html/2018/04/aa29377-16/aa29377-16.html.

[9] B. Degrange , G. Fontaine, *Introduction to high-energy gamma-ray astronomy*. Comptes Rendus Physique Vol. 16, August-September 2015. Available at https://www.sciencedirect.com/science/article/pii/S1631070515001292.

[10] CTA website. *How CTA works*. Available at: https://www.cta-observatory.org/about/how-cta-works/.

[11] Cherenkov Telescope Array Observatory Gallery, *Cherenkov Effect*. Available at https://www.flickr.com/photos/cta_observatory/45643242354/in/album-72157673853528865/

[12] B. M. Gaensler, P. O. Slane, *The Evolution and Structure of Pulsar Wind Nebulae*, Annu. Rev. Astronomy & Astrophysics 2006. Available at: https://arxiv.org/abs/astro-ph/0601081.

[13] TeVCat Catalogue. http://tevcat.uchicago.edu.

[14] O. Hamil, J.R. Stone et. al. *Braking Index of Isolated Pulsars*. Available at https://arxiv.org/abs/1608.01383.

[15] C.A. Faucher-Giguère, V.M. Kaspi, *Birth and evolution of isolated radio pulsars*. Available at https://arxiv.org/pdf/astro-ph/0512585.pdf.

[16] M. Mayer et al. *Predicting the X-ray flux of evolved pulsar wind nebulae based on VHE gamma-ray observations*. Available at https://arxiv.org/abs/1202.1455.

[17] R. Trotta et. al, *Constrains on Cosmic-Ray propagation models from a global bayesian analysys*. Available at: https://iopscience.iop.org/article/10.1088/0004-637X/729/2/106.

[18] H.E.S.S. Collaboration *The H.E.S.S. Galactic Plane Survey*, Astronomy & Astrophysics **612** A1 (2018). Available at: https://www.aanda.org/articles/aa/abs/2018/04/aa32098-17/aa32098-17.html.

[19] CSIRO website. *About ATNF*. Available at: https://www.csiro.au/en/Research/Facilities/ATNF/About-ATNF.

[20] J.H. Taylor, R.N. Manchester and A.G. Lyne, *Catalog of 558 Pulsars*, 1993, ApJS, 88, 529-568. Available at: https://ui.adsabs.harvard.edu/abs/1993ApJS...88..529T/abstract.

[21] ATNFPULSAR - ATNF Pulsar Catalogue. Available at https://heasarc.gsfc.nasa.gov/W3Browse/radio-catalog/atnfpulsar.html.

[22] Manchester, R. N., Hobbs, G.B., Teoh, A. & Hobbs, M., AJ, 129, 1993-2006 (2005). Available at: https://ui.adsabs.harvard.edu/abs/2005AJ....129.1993M/abstract.

[23] TeVCat2.0 Catalogue. http://tevcat2.uchicago.edu.

[24] A. U. Abeysekara et al. *Extended gamma-ray sources around pulsars constrain the origin of the positron flux at Earth*. Available at: https://arxiv.org/abs/1711.06223.

[25] W. R. Webber, *A New Estimate of the Local Interstellar Energy Density and Ionization Rate of Galactic Cosmic Cosmic Rays*. Available at: https://iopscience.iop.org/article/10.1086/306222.